Banp regulates DNA damage response and chromosome segregation during the cell cycle in zebrafish retina

Swathy Babu, Yuki Takeuchi, and Ichiro Masai[#]

Developmental Neurobiology Unit, Okinawa Institute of Science and Technology Graduate University (OIST)
1919-1 Tancha, Onna, Okinawa, Japan

Correspondence should be addressed: masai@oist.jp

Keywords: Banp, DNA damage, chromosome segregation, cell cycle, cenpt, ncapg, tp53

Word Count for Introduction/Results/Discussion: 6068

Abstract

Btg3-associated nuclear protein (Banp) was originally identified as a nuclear matrix-associated protein and it functions as a tumor suppressor. At molecular level, Banp regulates transcription of metabolic genes via a CGCG-containing motif called the Banp motif. However, its physiological roles in embryonic development are unknown. Here we report that Banp is indispensable for DNA damage response and chromosome segregation during mitosis. Zebrafish *banp* mutants show mitotic arrest and apoptosis in developing retina. We found that DNA replication stress and tp53-dependent DNA damage responses were activated to induce apoptosis in *banp* mutants, suggesting that Banp is required for integrity of DNA replication and DNA damage repair. Furthermore, in *banp* mutants, chromosome segregation was not smoothly processed from prometaphase to anaphase, leading to a prolonged M-phase. Our RNA- and ATAC-sequencing identified 31 candidates for direct Banp target genes that carry the Banp motif. Interestingly, two chromosome segregation regulators, *cenpt* and *ncapg*, are included in this list. Thus, Banp directly regulates transcription of *cenpt* and *ncapg* to promote chromosome segregation during mitosis. Our findings provide the first *in vivo* evidence that Banp is required for cell-cycle progression and cell survival by regulating DNA damage responses and chromosome segregation during mitosis.

(197 words)

Introduction

The vertebrate retina is composed of six major classes of neurons and one type of glia, namely retinal ganglion cells (RGCs), three types of interneurons (amacrine cells, bipolar cells, and horizontal cells), two types of photoreceptors (rods and cones), and Müller glia These retinal cells are assembled to form the neural circuit responsible for phototransduction and visual processing (Dowling, 2012). During development, retinal progenitor cells are multipotent and give rise to all seven retinal cell types in response to extrinsic and intrinsic cues (Boije et al., 2014). In addition, retinal neurogenesis is spatially and temporally regulated among vertebrates. In zebrafish, neurogenesis starts in the ventro-nasal retina at 25 h post-fertilization (hpf) and then spreads into the entire neural retina by 72 hpf (Hu and Easter, 1999; Masai et al., 2000). In general, early-born post-mitotic cells differentiate into RGCs and cone photoreceptors, followed by amacrine cells, bipolar cells, and horizontal cells, and late-born cells differentiate into rod photoreceptors and Müller glia, indicating stage-dependent retinal histogenesis.

Another important characteristic of retinal development is that retinal neurogenesis is linked to cell-cycle regulation. In zebrafish, cell-cycle length of retinal progenitor cells is around 32–49 h during 6 to 25 hpf, but shortened to 8–10 h once retinal neurogenesis starts at 25 hpf (Li et al., 2000), suggesting that activation of cell-cycle progression is associated with neurogenesis. It is generally accepted that active cell proliferation may increase DNA replication errors, which induces DNA replication stress and subsequent DNA damage (Berti et al., 2020; Blackford and Jackson, 2017; Waterman et al., 2020). Thus, DNA damage response is essential to ensure genomic integrity (Murga et al., 2009). Otherwise, retinal progenitor cells undergo cell-cycle arrest or apoptosis. Consistently, in zebrafish, retinal apoptosis occurs in the absence of DNA damage response regulators such as DNA damage-binding protein 1 (DDB1) (Hu et al., 2015), Fanconi anemia group D2 (Fancd2) (Liu et al., 2003), and Ku80 (Xrcc80) (Bladen et al., 2005). We also showed that retinal apoptosis occurs in zebrafish *prim1* mutants, in which DNA replication stress is chronically elevated. In this mutant, a central regulator of the DNA replication checkpoint, Ataxia telangiectasia-mutated (ATM) and Rad3-related (ATR), is activated, which subsequently activates DNA damage response regulators, ATM and Chk2, leading to tp53-mediated apoptosis. Thus, DNA replication checkpoint and DNA damage response function as safeguards to

ensure integrity of retinal cell proliferation and neurogenesis (Yamaguchi et al., 2008). However, it remains to be seen how the DNA damage response pathway is integrated into retinal cell proliferation and neurogenesis.

BTG3-associated nuclear protein (Banp) (also known as Scaffold/matrix attachment region binding protein 1 (SMAR1)) was identified as a nuclear protein that binds to the matrix-associated region (MAR) of the β-locus of murine T cell receptors (Birot et al., 2000; Chattopadhyay et al., 2000). MARs are often found near gene promoters (Scheuermann and Garrard, 1999) and constitute a periodic loop domain, through which chromosomal DNA is topologically organized inside the nucleus (Blasquez et al., 1989; Hart and Laemmli, 1998). Very recently, it was reported that Banp binds to the nucleotide sequence TCTCGCGAGA, called the "Banp motif", which is enriched near the transcription initiation site of CpG island promoters, and regulates gene transcription in a DNA methylation-dependent manner. Banp promotes transcription of essential metabolic genes in pluripotent stem and terminal differentiated neuronal cells in humans and mice (Grand et al., 2021). Furthermore, Banp functions as a tumor suppressor (Kaul et al., 2003; Kaul-Ghanekar et al., 2005). In humans, the *banp* gene is located on chromosome 16q24, the genomic region of which often suffers from loss-of-heterozygosity in various tumors (Tsuda et al., 1994; Wang et al., 1999). Banp interacts with tumor suppressor tp53 to modulate its functions (Kaul et al., 2003; Pavithra et al., 2009; Sinha et al., 2012; Sinha et al., 2010). Overexpression of Banp suppresses cancer growth (Bhagat et al., 2018; Liu et al., 2014; Taye et al., 2018). However, these cellular functions of Banp were proposed mostly from *in vitro* studies, and genetic deletion of *banp* was reportedly unsuccessful (Grand et al., 2021), whereas *banp* knockout mice show embryonic lethality (Chemmannur et al., 2015), which makes *in vivo* analysis difficult. Thus, physiological functions of Banp are still unknown.

In this study, we identified zebrafish *banp* mutants, which show mitotic arrest and apoptosis in the developing retina. DNA replication checkpoint and tp53-dependent DNA damage response are activated to induce apoptosis in *banp* mutant retinas. Thus, Banp is required for integrity of DNA replication and DNA damage repair. Furthermore, live imaging revealed that chromosome segregation fails to proceed smoothly during mitosis in *banp* mutants, resulting in a prolonged M-phase. Our RNA-sequencing and ATAC-sequencing enabled us to identify 31 candidates for direct Banp target genes that

carry the Banp motif near their promoters. Interestingly, two chromosome segregation regulators, *cenpt* and *ncapg*, are included in this list. Thus, Banp directly regulates the transcription of *cenpt* and *ncapg* to promote chromosome segregation during mitosis. Taken together, these data suggest that Banp is required for cell-cycle progression and cell survival in zebrafish retinas by regulating DNA damage response and chromosome segregation during mitosis.

Results

Zebrafish *rw337* mutants show mitotic cell accumulation and cell death in the retina after 2.5 dpf

We performed large-scale mutagenesis using zebrafish and identified a zebrafish mutant, *rw337*. *rw337* mutants have smaller eyes and a smaller optic tectum at 4 days post-fertilization (dpf) (Fig. 1A). Around 6–7 dpf, *rw337* mutants die, indicating a lethal mutation. Next, we examined retinal phenotypes (Fig. 1B). At 1.5 dpf, the retina consists of retinal progenitor cells and early differentiating neurons. There was no difference in retinal morphology between *rw337* mutants and wild-type siblings. However, at 2 dpf, mitotic-like round cells had accumulated in the apical region of the retina in *rw337* mutants, indicating mitotic arrest. At 2.5 dpf, in wild-type retinas, three nuclear layers, the RGC layer, the inner nuclear layer (INL) and the outer nuclear layer (ONL), and two plexiform layers, the inner plexiform layer (IPL) and the outer plexiform layer (OPL), had formed. In *rw337* mutants, only the RGC layer was observed; however, many pyknotic nuclei were observed in the outer retinal region. At 3 dpf, the RGC layer, IPL and INL appeared in *rw337* mutants. However, pyknotic nuclei were densely packed in the outer region of *rw337* mutant retinas. At 4 dpf, most dead cell debris had decreased in *rw337* mutants. The RGC layer, IPL, and INL were formed; however, no ONL was observed, despite very small, patchy photoreceptor-like cells. At 3 and 4 dpf, the ciliary marginal zone (CMZ), where retinal stem and progenitor cells are located, was observed in *rw337* mutants. Thus, RGCs differentiate, but mitotic arrest and cell death occur after 2.5 dpf in *rw337* mutants.

Next, we examined neuronal differentiation in *rw337* mutants at 4 dpf. The transgene *Tg[ath5:GFP]* drives GFP expression in RGCs (Fig. 1-figure supplement 1A) (Masai et al., 2000). Pax6 is strongly expressed in amacrine cells and weakly in RGCs (Fig. 1-figure supplement 1C) (Macdonald and Wilson, 1997). Prox1 is expressed in bipolar cells and horizontal cells (Fig. 1-figure supplement 1E) (Jusuf and Harris, 2009). zpr1 antibody labels double cone photoreceptors (Fig. 1-figure supplement 1G) (Larison and Bremiller, 1990). Anti-Gluta

mine synthetase (GS) antibody labels Müller cells (Fig. 1-figure supplement 1I) (Peterson et al., 2001). We observed that all these markers are expressed in *rw337*

mutants (Fig. 1-figure supplement 1B, 1D, 1F, 1H, 1J). However, the numbers of strong Pax6+ cells and GS+ cells were decreased in *rw337* mutants (Fig. 1-figure supplement 1D, 1J), suggesting that amacrine cells and Müller cells were reduced. Prox1+ cells were misplaced and less numerous in *rw337* mutants, suggesting that horizontal and bipolar cells are reduced (Fig. 1-figure supplement 1F). zpr1+ cells were not detected, except for a small patch of zpr1+ cells in the ventral retina, where photoreceptor differentiation initially occurs, in *rw337* mutants (Fig. 1-figure supplement 1H), suggesting that most cone photoreceptors fail to differentiate. Anti-PCNA antibody labels retinal stem and progenitor cells in the CMZ (Fig. 1-figure supplement 1K), which was not affected in *rw337* mutants (Fig. 1-figure supplement 1L). Phalloidin labeling shows IPL and OPL in wild-type retinas (Fig. 1-figure supplement 1M). *rw337* mutants showed IPL, but not OPL (Fig. 1-figure supplement 1N), which is consistent with zpr1 labeling (Fig. 1-figure supplement 1H). Thus, retinal stem and progenitor cells are maintained. RGCs do differentiate; however, amacrine cells, horizontal cells, bipolar cells, and Müller cells are decreased in number and photoreceptors fail to differentiate in *rw337* mutants.

***rw337* mutant gene encodes Banp**

We mapped the *rw337* mutation to zebrafish chromosome 25 (Fig. 1C). Two polymorphic markers, 070702B and zC93F2D, restricted the genomic region encompassing *rw337* mutation, in which only four candidate genes: *BTG3-associated nuclear protein* (*banp*); *programmed cell death 2-like* (*pdcd2l*); *carboxylesterase 2b* (*ces2b*); *protein disulfide isomerase family A, member 3* (*pdia3*), were annotated. We cloned all these cDNAs from mRNA prepared from *rw337* homozygous mutants, sequenced them, and found that a part of the intron sequence between exons 4 and 5 (intron 4/5) failed to be spliced out of the *banp* cDNA (Fig. 1D). A nucleotide T at the exon-intron junction of exon 4 is converted to G, which results in an alteration of the donor splice site of exon 4 from GT to GG. This mutation leads to the abnormal insertion of a 52-bp intron sequence after exon 4, resulting in a premature stop codon in *banp* cDNA (Fig. 1D). The *banp* gene encodes a protein containing a coiled-coil domain, a BEN domain and a DNA-binding domain, which includes a MAR-binding domain (Fig. 1E). Overall, zebrafish Banp protein shows high similarity

to those of humans and mice, especially in the BEN domain (Fig. 1-figure supplement 2). This mutation is predicted to generate nonfunctional, truncated Banp protein in *rw337* mutants (Fig. 1E). There was no mutation in the other three genes in *rw337* mutants, suggesting that the *rw337* mutant gene encodes Banp.

To confirm that the loss of Banp causes retinal phenotypes in *rw337* mutants, we carried out three sets of experiments. First, we examined another nonsense mutation allele, $banp^{sa12976}$, which has a premature stop codon in exon 4 (Fig. 1-figure supplement 3A). Homozygous $banp^{sa12976}$ mutant embryos and trans-heterozygous $banp^{rw337}$; $banp^{sa12976}$ mutants phenocopied *rw337* mutants (Fig. 1-figure supplement 3B). Second, we inhibited Banp using ATG-morpholino antisense oligos against Banp (banp MO). We confirmed MO specificity, because banp MO inhibited translation of mRNA encoding C-terminal EGFP-tagged wild-type Banp (banp(wt)-EGFP), whereas the control, 5-mismatch banp MO (banp 5misMO) did not (Fig. 1-figure supplement 4A and 4B). *banp* morphants phenocopied *rw337* mutants (Fig. 1F). Third, we overexpressed wild-type Banp in $banp^{rw337}$ mutants. We injected mRNA encoding Banp(wt)-EGFP into wild-type embryos at the one-cell stage. In the developing retinas, Banp(wt)-EGFP protein was localized in the nuclei during interphase, whereas it spread into the whole cell region during mitosis (Fig. 1-figure supplement 4C and 4D), confirming nuclear localization of zebrafish Banp. We expressed Banp(wt)-EGFP, N-terminal EGFP tagged wild-type (EGFP-Banp(wt)) and the *rw337* mutant form of Banp (EGFP-Banp(rw337)) in wild-type retinas. Only EGFP-Banp(rw337) was not stably maintained (Fig. 1-figure supplement 4E), suggesting that the mutant form of Banp protein is degraded, probably by nonsense mutation decay. Finally, overexpression of Banp(wt)-EGFP rescued retinal phenotypes in *rw337* mutants at 2 dpf, but overexpression of EGFP-Banp(rw337) did not (Fig. 1G). Taken together, retinal phenotypes of *rw337* mutants are caused by the loss of Banp.

***banp* mRNA is prominently expressed in the developing CNS of zebrafish**

We examined *banp* mRNA expression by *in-situ* hybridization (Fig. 1-figure supplement 5A). *banp* mRNA shows ubiquitous expression from the one-cell stage to the 21-somite stage, suggesting maternal and zygotic expression. mRNA was restricted to the brain, including the retina at 30 and 48 hpf. Frontal sections show that mRNA is

expressed in neural retina at 24 hpf, but restricted in the CMZ at 48 hpf, suggesting that retinal progenitor cells express *banp* mRNA (Fig. 1-figure supplement 5B). In addition to the brain and retinas, *banp* mRNA expression was observed in fin and notochord at 48 hpf and in neuromasts of the lateral line after 72 hpf. *banp* mRNA expression was not detected in *banp*^{rw337} homozygous mutants at 3 dpf (Fig. 1-figure supplement 5C), suggesting nonsense mutation-mediated decay. Thus, *banp* mRNA is prominently expressed in the developing brain in zebrafish.

banp mutants show cell cycle arrest followed by cell death of retinal progenitor cells

Although retinal progenitor cells produce RGCs in *banp* ^{rw337} mutant retinas, the number of other neurons, especially photoreceptors, was decreased at 4 dpf (Fig. 1-figure supplement 1). Indeed, mitotic-like round cells and pyknotic nuclei were accumulated in the outer region of *banp*^{rw337}mutant retinas from 2 to 3 dpf (Fig. 1B), suggesting that mitotic arrest and cell death eliminate retinal neurons. Accordingly, we performed TdT-mediated dUTP Nick End Labeling (TUNEL), which visualizes apoptosis. TUNEL+ cells were rarely observed in wild-type retinas throughout the stages from 29 to 101 hpf, as well as in *banp*^{rw337}mutant retinas at 24 hpf (Fig. 2A). However, in *banp*^{rw337}mutants, TUNEL+ cells appeared in the neural retina at 53 hpf, and became more localized to the outer retina at 77hpf (Fig. 2A) and to the interface between the central retina and the CMZ at 77 and 101 hpf (Fig. 2A). After 53 hpf, the number of TUNEL+ cells was significantly higher in *banp* ^{rw337} mutants than in wild-type siblings (Fig. 2C). Thus, retinal cells undergo apoptosis in *banp*^{rw337}mutants. Next, we examined mitosis by labeling with anti-phosphorylated (Ser-10) Histone H3 (pH3) antibody, which labels mitotic cells in pro-metaphase (Prigent and Dimitrov, 2003) (Fig. 2B). The number of pH3+ cells did not differ between wild-type and *banp*^{rw337}mutant retinas at 24 hpf. However, pH3+ cells were markedly increased and located at the apical surface of the neural retina in *banp*^{rw337}mutant retinas at 53 hpf (Fig. 2B), suggesting mitotic arrest. At 77 and 101 hpf, pH3+ cells disappeared from the central retina, but still were accumulated in the CMZ in *banp*^{rw337} mutants (Fig. 2B). The number of pH3+ cells in *banp* ^{rw337} mutant retinas increased transiently at 53 hpf, and then decreased, but was

still significantly higher than that of wild-type sibling retinas after 77 hpf because of accumulation of pH3+ cells at the CMZ (Fig. 2D).

To clarify how mitotic arrest and apoptosis are induced during retinal cell proliferation and neurogenesis in *banp*^{rw337} mutants, we examined BrdU incorporation and ath5:EGFP expression at 48 hpf (Fig. 2-figure supplement 1A and 1B). The percentage of BrdU+ area to total retinal area did not differ significantly between wild-type siblings and *banp*^{rw337} mutants (Fig. 2-figure supplement 1C), whereas the percentage of ath5:EGFP+ area to the total retinal area was slightly, but significantly lower in *banp*^{rw337} mutants than in wild-type siblings (Fig. 2-figure supplement 1C), suggesting that retinal neurogenesis is slightly reduced in *banp*^{rw337} mutants at 48 hpf, probably due to mitotic arrest or apoptosis.

Next, we examined the spatial position of mitotic arrest and apoptosis at 48 hpf by labeling with anti-pH3 and anti-activated caspase 3 antibodies (Fig. 2-figure supplement 1D and 1E). Both caspase 3+ and pH3+ cells were increased in *banp*^{rw337} mutants (Fig. 2-figure supplement 1F). Furthermore, caspase 3+ cells were mostly located in the intermediate zone of the neural retina along the apico-basal axis, whereas pH3+ cells were localized at the apical surface of the neural retina (Fig. 2-figure supplement 1G), suggesting that apoptosis occurs mostly in retinal progenitor cells undergoing G1 or S phase, or differentiating neurons. Next, we examined whether apoptosis occurs in early differentiating retinal neurons, using double labeling with anti-activated caspase 3 antibody and ath5:EGFP (Fig. 2-figure supplement 1H). The percentage of ath5:EGFP- and caspase 3-double-positive cells to the total number of caspase 3+ cells was 9.44±13.1% in *banp* mutants at 48 hpf and higher than that of wild-type siblings (0.00±0.00%), although the difference was not significant (Fig. 2-figure supplement 1I). Next, we examined whether apoptosis occurs in mature retinal neurons. HuC/D is expressed in maturing neurons (Park et al., 2000). At 48 hpf, anti-HuC/D antibody labeled RGCs in zebrafish (Fig. 2-figure supplement 1J). The fraction of caspase 3- and HuC/D-double-positive cells in the total caspase 3+ cells was almost zero in both wild-type and *banp*^{rw337} mutants (Fig. 2-figure supplement 1K), suggesting that apoptosis does not occur in maturing retinal neurons. Taken together, in *banp*^{rw337} mutants, retinal progenitor cells undergo mitotic arrest at 48 hpf. On the other hand, apoptosis is induced in retinal progenitor cells at G1 or S-phase or in newly

differentiating retinal neurons, although apoptosis in newly differentiating retinal neurons is minor (Fig. 2-figure supplement 1L). Since mitotic arrest was transiently observed at 53 hpf (Fig. 2B), but apoptosis continues in the central retina of *banp*^{rw337} mutants after 53 hpf (Fig. 2A), it is likely that apoptosis occurs following mitotic arrest (Fig. 2E and 2F).

tp53 pathway mediates retinal apoptosis in *banp* mutants

To understand molecular mechanisms of mitotic arrest and apoptosis in *banp*^{rw337} mutants, we identified differentially expressed mRNAs by RNA-seq analysis. We prepared mRNA from 48-hpf wild-type siblings and *banp*^{rw337} mutants. Illumina sequencing generated more than 50 million paired-end reads from cDNA libraries. 27,771 protein-coding genes were detected. Among them, 258 genes were upregulated, and 81 genes were downregulated in *banp*^{rw337} mutants (Fig. 3A). The top 15 upregulated genes were enriched regulators of tp53 dependent-DNA damage response (Fig. 3B). Quantitative RT-PCR revealed that four tp53 target genes: *p21(cdkn1a)*, *puma (bbc3)*, *ccng1*, and *mdm2* are significantly upregulated in *banp*^{rw337} mutants (Fig. 3C). Western blotting showed that full length tp53 (FL tp53) protein is stabilized and more than 11 fold higher in *banp*^{rw337} mutants than in wild type (Fig. 3D and 3E). We previously showed that the ATR/ATM-Chk2-tp53 DNA damage pathway induces retinal apoptosis in zebrafish (Yamaguchi et al., 2008). Indeed, mRNA expression of ATR and ATM was upregulated in *banp*^{rw337} mutants (Fig. 3F). So, we examined whether retinal apoptosis depends on tp53 in *banp*^{rw337} mutants. Injection of tp53 antisense morpholino (tp53 MO) completely inhibited retinal apoptosis in *banp*^{rw337} mutants at 48 hpf (Fig. 3G and 3H). However, retinal apoptosis reappeared in *banp*^{rw337} mutants injected with tp53 MO at 72 hpf (Fig. 3G), although there was no statistical difference in apoptotic cell number between wild-type and *banp*^{rw337} mutant retinas at 72 hpf (Fig. 3H). Thus, retinal apoptosis in *banp*^{rw337} mutants depends on tp53, although it is possible that some tp53-independent mechanism induces retinal apoptosis after 48 hpf.

Transcription of Δ113-tp53 is preferentially elevated in *banp* mutants

RNA-seq analysis showed upregulation of tp53 mRNA (Fig. 3B); however, surprisingly, quantitative RT-PCR showed that the mRNA level of FL tp53 is not significantly different between *banp*^{rw337} mutants and wild-type siblings at 48 hpf (Fig. 4A). There are several isoforms of tp53 protein (Joruiz et al., 2020; Joruiz and Bourdon, 2016). Importantly, in zebrafish, the isoform Δ113tp53 is generated from the alternative transcription start site in intron 4. Δ113tp53 preferentially activates the transcription of target genes related to cell-cycle arrest to promote DNA repair and cell survival, whereas FL tp53 preferentially activates transcription of target apoptotic genes to eliminate severely DNA-damaged cells (Gong et al., 2015; Gong et al., 2020). Differential expression of tp53 isoforms is thought to regulate the balance between cell survival and apoptosis in response to DNA damage. Indeed, quantitative RT-PCR confirmed that only Δ113tp53 was upregulated in *banp*^{rw337} mutants (Fig. 4A). ATAC-seq revealed that a genomic region in intron 4 of tp53 is specifically open in *banp*^{rw337} mutants but not in wild-type siblings (Fig. 4B, ATAC-seq). Consistently, transcription of the Δ113tp53 mRNA was specifically activated in *banp*^{rw337} mutants, but not in wild-type siblings (Fig. 4B, RNA-seq). Thus, the internal promoter at intron 4 (Chen et al., 2009; Chen et al., 2005) is specifically activated in *banp*^{rw337} mutants (Fig. 4B). These data raise the possibility that the lack of Banp increases DNA replication stress and promotes an accumulation of DNA damage, resulting in activation of ATR and ATM, which stabilize FL tp53, such that FL tp53 triggers Δ113tp53 transcription in *banp*^{rw337} mutants (Fig. 4G).

DNA double-strand breaks accumulate in *banp* mutant retinas

To examine whether DNA damage is increased due to loss of Banp functions, we labeled 48-hpf retinas with anti-γ-H2AX antibody, which marks DNA double-strand breaks (Rogakou et al., 1998; Shroff et al., 2004). The number of γ-H2AX+ cells increased in both *banp*^{rw337} mutant (Fig. 4C, 4F) and *banp* morphant retinas (Fig. 4-figure supplement 1A, 1B), confirming an accumulation of DNA damage in the absence of Banp. Next, to determine how DNA damage is induced in *banp*^{rw337} mutants, we examined the fraction of S-phase cells, mitotic cells, and post-mitotic neurons in γ-H2AX+ retinal cells in *banp*^{rw337} mutants at 48 hpf. First, wild-type and *banp*^{rw337} mutant retinas carrying the transgene *Tg[ath5:EGFP]* were labeled with anti-BrdU and

anti-γ-H2AX antibodies (Fig. 4-figure supplement 1C). The fraction of γ-H2AX+ cells increased in *banp*^{rw337} mutant retinas, whereas the fraction was almost zero in wild-type sibling retinas (Fig. 4-figure supplement 1D). Next, we compared the fraction of BrdU+ cells between the total retinal cells and γ-H2AX+ retinal cells in *banp*^{rw337} mutants (Fig. 4-figure supplement 1E). The BrdU+ fraction was significantly higher in γ-H2AX+ cells than in the total retinal cells (Fig. 4-figure supplement 1F), indicating that S-phase fraction is 4.3 fold higher in DNA damaged retinal cells than in the total retinal cells, in *banp*^{rw337} mutants. Thus, DNA double-strand breaks are abnormally induced or fail to be repaired in retinal progenitor cells undergoing S phase. Next, we examined the fraction of ath5:EGFP+ cells (Fig. 4-figure supplement 1G). There was no significant difference in ath5:EGFP+ cell fraction between the total retinal cells and γ-H2AX+ retinal cells in *banp*^{rw337} mutants (Fig. 4-figure supplement 1H). Finally, we determined the fraction of mitotic cells by labeling with anti-pH3 and anti-γ-H2AX antibodies in *banp*^{rw337} mutant retinas at 48 hpf (Fig. 4-figure supplement 1I). There is no significant difference in pH3+ cell fraction between the total retinal cells and γ-H2AX+ retinal cells (Fig. 4-figure supplement 1J). Although DNA damage may occur in post mitotic neurons and mitotic cells in *banp*^{rw337} mutants, it is likely that most DNA damage is introduced in S-phase of retinal progenitor cells in the absence of Banp.

It is generally accepted that tp53 promotes DNA damage repair or eliminates DNA-damaged cells via apoptosis, so we expected that tp53 knockdown may enhance accumulation of DNA damage in *banp*^{rw337} mutants. However, compared with standard-MO injection control (n=120.8±60.6/section), the injection of FL tp53-MO significantly reduced the number of γ-H2AX+ cells in *banp*^{rw337} mutant retinas (n=55.9±15.9/section) at 48 hpf (Fig. 4C, 4F). The injection of Δ113tp53-MO mildly reduced the number of γ-H2AX+ cells (n=85.4±15.2/section); however, the difference was not significant (Fig. 4C, 4F). It is likely that tp53 or Δ113tp53 does not repair DNA damage in *banp*^{rw337} mutants, but rather it may enhance DNA damage in *banp*^{rw337} mutants. Thus, Banp normally suppresses DNA replication stress upstream of tp53, or promotes DNA damage repair in concert with tp53 (Fig. 4G).

In addition, we investigated whether retinal apoptosis and mitotic arrest in *banp*^{rw337} mutants depend on FL tp53-MO or Δ113tp53-MO. Compared with Standard-MO injection control (n=174.7±30.5/section), retinal apoptosis was completely

inhibited by FL tp53-MO in *banp*^{rw337} mutant retinas (n=0.50±0.58/section) at 48 hpf (Fig. 4C, 4D). However, inhibition of apoptosis in *banp*^{rw337} mutant retinas by Δ113tp53-MO was significant, but ineffective (n=58.00±11.0/section) (Fig. 4C, 4D). This result is consistent with previous reports proposing that Δ113tp53 preferentially activates transcription of target genes related to cell-cycle arrest rather than apoptosis (Gong et al., 2015; Gong et al., 2020). However, compared with Standard-MO injection controls (n=376.6±74.8/section), the number of pH3+ cells in *banp*^{rw337} mutants was significantly decreased by FL tp53-MO (n=262.4±68.3/section) (Fig. 4C, 4E). However, the number of pH3+ cells was still higher in *banp*^{rw337} mutant retinas injected with FL tp53-MO than in wild-type control retinas injected with FL tp53-MO. The injection of Δ113tp53-MO did not significantly rescue mitotic arrest in *banp*^{rw337} mutants (n=303.8±46.6/section) (Fig. 4C, 4F). These data suggest that mitotic arrest in *banp*^{rw337} mutants is mostly mediated by a tp53-independent mechanism.

Banp is required for the expression of chromatin segregation genes

Mitotic arrest in *banp*^{rw337} mutants is independent of tp53. RNA-seq analysis revealed that two chromosomal segregation regulators, *cenpt* and *ncapg*, are downregulated in *banp*^{rw337} mutants at 48 hpf (Fig. 3B). Cenpt and Ncapg are essential for chromatin segregation (Hung et al., 2017; Seipold et al., 2009; Zhang et al., 2018). Quantitative RT-PCR confirmed their downregulation in *banp*^{rw337} mutants and *banp* morphants (Fig. 5A, 5C). Furthermore, ATAC-seq revealed that chromatin accessibility is decreased near the transcription start site (TSS) of both genes in *banp*^{rw337} mutants, leading to reduction of transcription activity (Fig. 5B, 5D). Thus, Banp is required for transcriptional activation of *cenpt* and *ncapg* genes. Interestingly, two independent chip-sequencing studies using Banp antibody revealed a specific binding site within 100 bp of the TSS of *cenpt* and *ncapg* genes in mice and humans (Grand et al., 2021; Mathai et al., 2016), suggesting that the requirement for Banp in *cenpt* and *ncapg* transcription is conserved in zebrafish, mice, and humans. Furthermore, using motif discovery software (HOMER), we discovered that TCTCGCGAGA, which was reported to be the Banp motif (Grand et al., 2021), is the most enriched motif in the closed chromatin region of *banp*^{rw337} mutants (Fig. 5E, Fig. 5-figure supplement 1A). Indeed, among 81 down-regulated genes in *banp*^{rw337} mutants (Fig. 3A), we identified the Banp motif near the

TSS of 31 genes (Fig. 5F and Supplementary table 1), 26 % of which was cell-cycle regulators (Fig. 5G, 5H) including *cenpt* and *ncapg* (Fig. 5I and 5J). However, we could not find the Banp motif in 258 upregulated genes. Furthermore, the Banp motif occurs upstream of the TSS of both *cenpt* and *ncapg* in mice and humans (Fig. 5-figure supplement 1B, 1C). Their Banp motif position is consistent with the previous report, that the Banp motif is not located at a constant distance from TSSs, but rather between 20 and 70 nucleotides upstream on both strands, and that the frequency of the Banp motif occurrence upstream of TSSs may correlate to a transcription rate of target genes (Mahpour et al., 2018) (Supplementary table 1). Taken together, it is likely that Banp directly regulates transcription of *cenpt* and *ncapg* via the Banp motif.

Chromosomal segregation is abnormal in *banp* mutants

Knockdown of Cenpt and Ncapg causes defects in chromosomal segregation during mitosis in zebrafish (Hung et al., 2017; Seipold et al., 2009). So, we conducted time-lapse imaging of mitosis in *banp*^{rw337} mutant retinas for 1-2 h from 48 to 54 hpf, using a transgenic line *Tg[h2afv:GFP; EF1α:mCherry-zGem]*, which visualizes cell-cycle phases (Mochizuki et al., 2014). In wild-type retinas injected with control banp 5misMO, chromatin starts to be condensed in prophase, kinetochores and a mitotic spindle appear in prometaphase, chromosomes are centrally aligned and start to be pulled toward the opposite poles by mitotic spindles in metaphase, sister chromatids move toward the opposite poles in anaphase, and chromosomes arrive at the opposite poles in telophase, whereupon cytokinesis starts (Fig. 6A, Video 1). The duration from prophase to telophase was 22.9±5.8 minutes (Fig. 6B). On the other hand, mitosis did not proceed smoothly in *banp* morphant retinas, especially from prophase to anaphase (Fig. 6A, Video 2). It took longer from chromosomal condensation in prophase to chromosomal alignment at the division plane in anaphase in *banp* morphant retinas (t=15 to t=46 in banp-MO, Fig. 6A). Aligned chromosomes were often dispersed during chromosomal segregation by the mitotic spindle (t=46 to t=64 in banp-MO, Fig. 6A), although all 28 cell divisions eventually completed cytokinesis in *banp* morphants. The duration from prophase to telophase was 49.2± 17.0 minutes and significantly longer in *banp* morphants (Fig. 6B). Thus, chromosomal segregation is abnormal during mitosis in the absence of Banp. Furthermore, we labeled 48-hpf retinas with anti-α-

tubulin and anti-pH3 antibodies to visualize the mitotic spindle and prometaphase chromosomes, respectively. In *banp*^{rw337} mutants, mitotic spindles are irregularly attached to less condensed and misaligned chromosome (Fig. 6C). The percentage of cells with abnormal mitosis was significantly higher in *banp*^{rw337} mutant retinas than those of wild-type siblings (Fig. 6D). These data suggest that the interaction between chromosomes and mitotic spindles is compromised in the absence of Banp, probably due to kinetochore attachment defects caused by lack of Cenpt and Ncapg. Thus, Banp regulates chromosomal segregation during mitosis.

Taken together, Banp plays essential roles in cell-cycle regulation in the zebrafish developing retina. During the S phase, Banp suppresses DNA replication stress and promotes DNA damage repair in concert with tp53-mediated DNA damage response. In the M phase, Banp promotes mitosis by activating the transcription of two chromosome segregation regulators, *cenpt* and *ncapg*, most likely via their Banp motifs (Fig. 7).

Discussion

Banp was initially identified as a nuclear matrix-associated protein and reported to function as a tumor suppressor (Malonia et al., 2011). Very recently, it was reported that Banp binds to the Banp motif enriched near the TSS of CpG island promoters and regulates transcription of metabolic genes (Grand et al., 2021). However, physiological functions of Banp during embryonic development remain to be discovered. In this study, we identified zebrafish *banp* mutants, in which retinal progenitor cells show mitotic arrest and subsequent apoptosis during embryonic development. RNA-seq analysis revealed that expression of tp53-dependent DNA damage response regulators is upregulated in *banp* mutants. In a non-stress condition, tp53 is degraded through ubiquitination by an E3-ubiqutin ligase, Mdm2, and subsequent actions of proteasomes, keeping its protein level very low (Oliner et al., 1993). On the other hand, under stress, such as DNA replication stalling or DNA double-strand breaks, ATR and ATM are activated and phosphorylate the N-terminal serine of tp53 (Saito et al., 2002; Tibbetts et al., 1999). This phosphorylation reduces the binding affinity of Mdm2 for tp53, resulting in stabilization of tp53 protein (Yadahalli et al., 2019). Indeed, the tp53 protein level is increased in *banp* mutants, and mRNA expression of ATR and ATM is also elevated. tp53 knockdown effectively suppresses retinal apoptosis in *banp* mutants. These data suggest that DNA replication stress is elevated in *banp* mutants, resulting in activation of tp53-dependent DNA damage response, which subsequently induces apoptosis of retinal progenitor cells.

It is generally accepted that tp53 has dual, but opposing roles: cell survival versus cell death in response to DNA replication stress and DNA damage (Chen, 2016). In the initial phase of the DNA damage response, tp53 binds to its alternative promoter located in intron 4 and activates transcription of an N-terminal truncated isoform Δ113-tp53, which preferentially activates transcription of target genes related to cell-cycle arrest for promoting DNA repair and cell survival (Chen et al., 2009). However, if DNA damage fails to be repaired, but accumulates chronically, FL tp53, in turn, activates transcription of apoptotic genes for eliminating DNA-damaged cells. Previous *in vitro* studies of human *banp* suggest that Banp physically interacts with tp53 to promote transcription of cell-cycle arrest genes and suppresses transcription of apoptotic genes, leading to promotion of its cell survival role (Jalota et al., 2005; Sinha et al., 2010).

Indeed, our quantitative RT-PCR showed that transcription of Δ113-tp53 is significantly elevated in *banp* mutants, whereas the mRNA level of FL tp53 is very low. RNA-seq and ATAC-seq also confirmed a higher level of transcription and chromatin accessibility of Δ113tp53 in *banp* mutants. These data suggest that Δ113tp53-mediated transcription is selectively activated in *banp* mutants. Thus, it is important to clarify the role of tp53, including Δ113tp53 in mitotic arrest in *banp* mutants, because pH3+ cells are markedly accumulated in *banp* mutant retinas prior to apoptosis. However, tp53-MO mildly inhibited accumulation of pH3+ cells in *banp* mutants. There is no significant difference in pH3+ cell accumulation between tp53-MO and Δ113tp53-MO, or between wild-type siblings and Δ113tp53-MO. So, these data suggest that the contribution of tp53 and Δ113tp53 to mitotic arrest in *banp* mutants seems to be minor, and that a tp53-independent pathway is responsible for mitotic arrest phenotypes. Our live imaging of mitosis in *banp* morphant retinas reveals that mitosis is significantly longer due to chromosome segregation defects; however, importantly, almost all mitoses are eventually completed in *banp* mutants, suggesting that accumulation of pH3+ cells in *banp* mutants is transient and depends mostly on prolonged mitosis, which is caused by chromosome segregation defects. At present, we have not observed S-phase arrest in *banp* mutants, because the fraction of BrdU+ cells in the total retinal region is not increased in *banp* mutants, although mRNA expression of a cdk inhibitor, *cdkn1a* (*p21*), is higher in *banp* mutants than in wild-type siblings. Taken together, we conclude that tp53 mainly mediates retinal apoptosis, and that its role in cell-cycle arrest is minor in *banp* mutants.

Labeling with anti-γ-H2AX antibody revealed that DNA damage is increased in retinal progenitor cells in *banp* mutants, suggesting that DNA damage is abnormally introduced or fails to be repaired in the absence of Banp. Importantly, the level of DNA damage in *banp* mutant retinas is not increased by either tp53-MO and Δ113tp53-MO, suggesting that tp53 does not repair DNA damage without Banp. There are two possible functions of Banp in DNA damage regulation. Banp may maintain the integrity of DNA replication. Banp functions as a transcription factor to regulate expression of essential metabolic genes in pluripotent stem cells and differentiating neurons (Grand et al., 2021). Therefore, Banp may promote transcription of DNA replication regulators. Our RNA-seq data identified 81 downregulated genes in *banp* mutants, compared to wild-

type siblings. Among them, 31 genes have a Banp motif near their TSSs and contain eight cell-cycle regulatory genes. It will be interesting to examine whether these Banp targets are involved in the activation of DNA replication stress in *banp* mutants. Another possibility is that Banp is required for DNA repair. A previous study using human *in vitro* culture cells revealed that Banp promotes HDAC6-mediated deacetylation of a DNA end joining protein Ku70, which is required for non-homologous end-joining repair (Chaudhary et al., 2014). Since Ku70 is recruited to the double-strand damage site after γ-H2AX accumulation, Ku70 is an interesting candidate. Since knockdown of Ku70 along with radiation-induced DNA damage markedly induces apoptosis in zebrafish embryos (Bladen et al., 2007), it will be interesting to investigate whether this scenario is the case in zebrafish.

In addition to the role of Banp in DNA replication stress and DNA repair mechanisms, mRNA expression of two important regulators of chromosome segregation, *ncapg* and *cenpt*, is significantly downregulated in *banp* mutants. ATAC-seq and RNA-seq confirmed that chromatin accessibility is decreased near the TSSs of these genes in *banp* mutants, suppressing transcription of these mRNAs. Our *de novo* motif enrichment study identified the Banp motif sequence, TCTCGCGAGA, as the most enriched motif of closed chromatin regions of downregulated genes. Thus, it is highly likely that Banp directly binds to the Banp motifs of both *ncapg* and *cenpt*, opens their chromatin, and promotes their transcription. Consistently, as reported in zebrafish *ncapg* and *cenpt* knockdown embryos (Hung et al., 2017; Seipold et al., 2009), chromosome segregation is compromised in mitosis of retinal progenitor cells in *banp* mutants, suggesting that Banp is an essential regulator of mitosis. Since a Banp motif is found in the promoter region of *ncapg* and *cenpt* in mice and humans, and Chip sequencing with Banp antibody validated TSS peaks of both *ncapg* and *cenpt* genes in humans and mice (Grand et al., 2021; Mathai et al., 2016), it will be interesting to confirm whether Banp regulates chromosome segregation during mitosis in mammals.

Lastly, we identified 26 candidates of Banp direct target genes, including *ncapg* and *cenpt*, which carry the Banp motifs near their TSSs, and show markedly decreased chromatin accessibility and transcription in the absence of Banp. This gene list will provide a useful starting point to investigate the Banp-mediated transcriptional network. It was reported that the binding of Banp to the Banp motif is dependent on DNA

methylation of the Banp motifs (Grand et al., 2021), suggesting that an epigenetic mechanism regulates Banp-mediated transcription. Thus, zebrafish *banp* mutants provide an excellent new model in which to study how epigenetic factors regulate cellular processes for embryonic development via the Banp motifs of CpG island promoter genes. In addition, Banp has been proposed as a tumor suppressor (Malonia et al., 2011). It is generally accepted that DNA methylation of essential genes is altered in cancer cells (Baylin et al., 2001), which is expected to modify a pattern of gene transcription through Banp motifs (Grand et al., 2021). It will be interesting to investigate how the Banp-mediated transcription profile is changed in cancer models of zebrafish. Future research on zebrafish *banp* mutants will provide more in-depth understanding of cancer growth and metastasis, as well as new insights into therapy development of tumors in human.

Material and Methods

Zebrafish strains and maintenance

Zebrafish (*Danio rerio*) were maintained using standard procedures (Westerfield, 1993). RIKEN Wako (RW) was used as a wild-type strain for mutagenesis in which *banp*^{rw337} was generated. Mapping of the *rw337* mutation and analysis of retinal phenotypes of *banp*^{rw337} mutants were carried out in the genetic background of WIK and Okinawa wild-type (oki), respectively. Two *banp* mutant alleles, *banp*^{rw337} and *banp*^{sa12976} were used. *banp*^{sa12976} was obtained from the Zebrafish International Resource Center (ZIRC, Eugene, OR, USA). Zebrafish transgenic lines, *Tg[h2afv:GFP]*$^{kca6/kca66}$ (Pauls et al., 2001), *Tg[EF1α:mCherry-zGem]*^{oki011} (Mochizuki et al., 2014) and *Tg[EF1α:mCherry-CAAX]*^{oki049} (Mochizuki et al., 2017) were used to visualize chromatin, S/G2/M phases and plasma membranes, respectively.

Ethics statement

All zebrafish experiments were carried out in accordance with the Okinawa Institute of Science and Technology Graduate School's Animal Care and Use Program, which is based on the National Research Council of the National Academy's Guide for the Care and Use of Laboratory Animals and has been accredited by the Association for Assessment and Accreditation of Laboratory Animal Care (AAALAC International). The OIST Institutional Animal Care and Use Committee approved all experimental protocols.

Zebrafish mutagenesis, mapping and cloning of the *banp* mutant gene

Mutagenesis, mapping, and cloning were performed as previously described (Masai et al., 2003). The polymorphic markers, 070702B and zC93F2D, shown below were designed and used for restricting the genomic region covering the *banp*^{rw337} mutation.

070702B forward: 5’-ACTTCTTATCAGGGCTGTGC-3’

070702B reverse: 5’-TCAGTCAAGAGCAGTGAGAG-3’

zC93F2D forward: 5’-TGGGATCTCTTTAAGTGAGTGAG-3’

zC93F2D reverse: 5’-TCCAACTATGTGGGTCAAACC-3’

Genotyping of *banp*^{rw337} mutant embryos

banp^{rw337} mutant phenotypes were difficult to distinguish until 2 dpf. Identification of homozygous mutant embryos at earlier time points was performed using PCR amplification of genomic regions using specific primers that enabled restriction digestion of only mutated sequence using MboII. Primers used, forward: 5'-CGATGTTGATATCCATCAGTCAGGCGATC-3'; reverse primer: 5'-GGTGCTGGTGTATAAATCACATGACCTATGGTCCTCTT-3'.

Acridine Orange staining

Larvae were incubated at 28°C, in 5 mg/mL Acridine Orange (AO) in E3 embryonic medium (5mM NaCl, 0.17mM KCl, 0.33mM $CaCl_2$, 0.33mM $MgSO_4$) for 30 min, protected from light. Embryos were rinsed in E3 medium and viewed with an epifluorescence microscope (SteREO Discovery, Zeiss) to identify live mutant embryos with dead cell accumulation.

***In situ* hybridization**

Whole-mount *in situ* hybridization of zebrafish embryos was performed as previously described (Xu et al., 1994). To prepare RNA probes, full-length cDNAs of zebrafish *banp* gene were amplified with PCR and sub-cloned into pBluescript II SK(+) vector (Stratagene/Agilent Technologies). Plasmids were digested with an appropriate restriction enzyme and used for DNA templates to make antisense or sense RNA probes. Digoxigenin-labeled RNA probes were generated by *in vitro* transcription using a DIG RNA Labeling Kit (Roche) and purified using Micro Bio-Spin® Chromatography Columns (BioRad). *In situ* hybridization signals in whole-mount embryos were detected using anti-DIG alkaline phosphatase (AP)-conjugated antibody (Roche) with an AP substrate, BM-Purple (Roche) and imaged using SteREO Discovery.V12 (ZEISS) microscope.

Rescue experiment of *banp* mutants with overexpression of wild-type Banp

The full-length coding region of the *banp* gene was amplified with PCR. To overexpress wild-type Banp protein, a DNA construct encoding zebrafish wild-type

Banp with an EGFP tag at the N-terminus or C-terminus, EGFP-banp(wt) or banp(wt)-EGFP, was prepared. A DNA construct encoding an N-terminal EGFP-tagged *rw337* mutant form of Banp, EGFP-Banp(rw337), was prepared as a negative control. These DNA constructs were subcloned into the pCS2 expression vector. Capped mRNA was generated in a standard *in vitro* transcription reaction using an SP6 polymerase (mMESSAGE mMACHINE™ SP6 Transcription Kit, Invitrogen). We performed mRNA injections in one-cell-stage embryos obtained from pair-wise crosses of *banp*^{rw337} heterozygous mutant male and female fish. At 2 dpf, embryos were used to determine their genotype with PCR and to identify homozygous mutants. Plastic sections were obtained to evaluate retinal phenotypes of *banp*^{rw337} mutant embryos injected with mRNA encoding banp(wt)-EGFP, or EGFP-banp(rw337). We also evaluated protein stability and nuclear localization of wild-type and *rw337* mutant form of Banp by live confocal imaging of wild-type retinas expressing banp(wt)-EGFP, EGFP-banp(wt), or EGFP-banp(rw337) at 24 hpf.

Morpholino injection

ATG morpholino antisense oligos for *banp* (banp MO) and its 5 mismatch *banp* MO (banp 5misMO) were designed as 5'-CCACTAAATCTTGCTCTGACATCAT-3' and 5'-CCtCaAAATgTTcCTCTcACATCAT-3', respectively. Morpholino antisense oligos for tp53 (tp53 MO) (5'-GCGCCATTGCTTTGCAAGAATTG-3') (Langheinrich et al., 2002), standard MO (STD MO) (5'-CCTCTTACCTCAGTTACAATTTATA-3') were used. To knock down Δ113tp53, morpholino antisense oligos for Δ113tp53 (Δ113tp53 MO; also referred to as MO6-tp53 in zebrafish database ZFIN) (5'-GCAAGTTTTTGCCAGCTGACAGAAG-3') was used (Chen et al., 2009). All MOs were injected into one-cell-stage eggs at 1 mM.

Histology

Plastic sectioning, immunostaining of cryosections, paraffin sectioning, and BrdU incorporation were performed as described previously (Imai et al., 2010), except that we injected BrdU solution into the yolk of embryos at 48 hpf instead of soaking embryos in 10mM BrdU solution. Anti- pH3 antibody (Cell signalling technology, 6G3, 9706; Sigma-Aldrich, 06-570), anti-Pax6 antibody (Covance; PRB-278P), zpr1 antibody

(ZIRC, Eugene, Oregon), anti-Prox1 antibody (GeneTex, GTX128354), anti-glutamine synthetase (GS) (Millipore, MAB302), anti-BrdU antibody (abcam, Ab6326), anti-PCNA (Sigma-Aldrich, P8825) were used at 1:500, 1:500, 1:100, 1:500, 1:100, 1:200, 1:200 dilutions, respectively. Nuclear staining was performed using SYTOX Green (Molecular Probes). Filamentous actin (F-actin) was stained using 0.1 mM rhodamine-conjugated phalloidin (Molecular Probes). Terminal deoxynucleotide transferase-mediated dUTP nick-end labeling (TUNEL) was performed using the In Situ Cell Death Detection Kit (Roche).

Whole-mount immunostaining with anti-α-tubulin antibody (Sigma-Aldrich; #T5168) to label the mitotic spindle was performed as follows. Homozygous mutant embryos were selected by AO staining, and fixed in 2% trichloroacetic acid (TCA) at room temperature (RT) for 3 h. Then embryos were washed three times in 1X PBST (PBS, 0.1 % tritonx100), and incubated in 0.2% trypsin for 4 min at 4°C to increase antibody permeabilization through the skin. Then, embryos were rinsed thrice with PBS. After embryos were re-fixed with 4% PFA for 5 min at 4°C, they were incubated in blocking solution (10% Goat serum in PBST) for 1 h at RT and transferred to 1% blocking solution with diluted anti-α-tubulin antibody at 1:1000 dilution for 2 days at 4°C. Embryos were washed with PBST four times for 15 min and then incubated with fluorescent conjugated anti-mouse antibody in 1% blocking solution in the dark for 2 days at 4°C. Next, all samples were washed in PBST three times for 15 min followed by glycerol storage at 4°C until imaging. Samples were imaged with a confocal microscope LSM 880 (Zeiss) followed by image analysis using IMARIS software (ver.9.1.2 Bitplane). Whole-mount immunostaining for anti-pH3, anti-γ-H2AX (GeneTex, GTX127342) (Sidi et al., 2008), anti-active caspase3 (BD Pharmingen, Clone C92-605), anti-HuC/D (Thermo Fisher, A-21271) (Sorrells et al., 2013) were performed as described previously (Imai et al., 2010). Images were scanned using an LSM710 confocal laser scanning microscope (Zeiss). Number of fluorescent-positive cells and percentage of fluorescence-positive area relative to the region of interest was calculated using original scanning images with IMARIS (Bitplane) and Zen (Zeiss) or Image-J (NIH) software, respectively.

RT-PCR

Total RNA was extracted from embryo heads at the indicated developmental stages using a Sepasol RNA I Super (Nacalai, Japan). cDNA synthesis was carried out from 500ng of RNA using Toyobo ReverseTra Ace® qPCR RT master mix with gDNA remover according to the manufacturer's instructions. Expression profiles of the genes listed below were analyzed with the specified primers using Luna® Universal qPCR Master Mix (NEB). Quantitative RT-PCR was performed using StepOnePlus (Applied Biosystems). The relative expression was calculated using ΔΔCt method with the reference gene ef1α. Primers used in qRT-PCR analysis; mdm2 (Wilkins et al., 2013), p21 (Stiff et al., 2016), FL tp53 and Δ113 tp53 (Chen et al., 2016), ef1α (McCurley and Callard, 2008).

Gene	**RT PCR-Forward primer**	**RT PCR-Reverse primer**
ccng1	ccctggagattgaggatcag	cacacaaaccaggtctccaa
mdm2	caggaggaggagaagcagtg	agggaaaagctgtccgactt
p21(cdkn1a)	aagcgcaaacagaccaacat	tcagctactggccggattt
FL tp53	tggagaggaggtcggcaaaatcaa	gactgcgggaacctgagcctaaat
Δ113 tp53	atatcctggcgaacatttggaggg	cctcctggtcttgtaatgtcac
Puma (bbc3)	ctgaggaggaccccacact	tctccagttctgccagtgc
cenpt	tcatgaggagattgtggaagatg	ggtgagctctgcgagttatt
ncapg	ctgatgtgagggagcctattt	gagtctgtttggcctccatta
atm	cctcaaggctgtggagaact	aggggattttctttacaccactc
atr	aggaacccaatctgccagt	gatgtccagtgccagctctc
ef1α	cttctcaggctgactgtgc	ccgctagcattaccctcc

Western blotting

Total 21 embryos were divided into 3 groups (each n=7) for 48 hpf wild-type and *banp*^{rw337} mutants, respectively. Heads were dissected in ice-cold E3 medium. Seven heads removed from each group were homogenized together in sample buffer (125 mM NaCl, 50 mM Tris-HCl pH 7.4, 0.5 mM EDTA, 1% Triton X-100, 1X Protease inhibitor) and used as one sample. Appropriate volumes of samples were diluted to provide equal protein amounts and used for SDS-PAGE (BIO-RAD, Mini-PROTEAN

TGX Gels). Western blot analysis was performed to 3 samples for wild-type and *banp*^{rw337} mutants, respectively, according to standard protocols using anti-tp53 antibody (GeneTex, GTX128135) at a 1:1000 dilution. β-actin protein level was evaluated by western blot analysis of rehybridized membranes with anti-β-actin antibody (Sigma, A5441) at a 1:5000 dilution, and used to normalize tp53 protein level for each sample. For secondary antibodies, horseradish peroxidase-conjugated anti-rabbit or anti-mouse IgG antibodies (Amersham, NA931 and NA934) were used. Enzyme activity was detected using Immunostar® LD (Wako) and luminescence was imaged and quantified using iBright 1500 (Thermo Fisher Scientific).

Live imaging

Banp-MO was injected into one-cell-stage eggs of *Tg[h2afv:GFP; EF1α: mCherry-zGem]* transgenic line. Banp-5misMO was used as a control. Two dpf embryos were anesthetized using 5% (v/v) Tricane (3-amino benzoic acid-ethylester) and mounted laterally using 1% low-melting agarose on a depression slide to image retinas without left or right preference. Time-lapse images were obtained every 1.1 min using a confocal laser scanning microscope LSM710 (Zeiss) with 40X0.8/1.0W Plane Apochromat lens. Data were evaluated using IMARIS software (ver.9.1.2 Bitplane) to calculate the time taken to complete each cell division.

RNA sequencing

Embryo heads were homogenized using a Polytron 1200E homogenizer (KINEMATICA) with TRIzol reagent (Invitrogen). RNA was isolated using a Direct-zol RNA Miniprep Kit (ZYMO RESEARCH) from three replicates of *banp*^{rw337} mutant and wild-type embryos at 48 hpf. Each sample contained a pool of 7 embryo heads. RNA isolation was followed by library preparation for sequencing using an NEBNext® Ultra™ II Directional RNA Library Prep Kit for Illumina® according to the manufacturer's instructions. 151-base paired-end sequencing was performed using a NovaSeq6000 SP. The quality of sequenced reads was evaluated with FastQC (Andrews, 2010) and adaptor trimming and quality filtering were done with fastp (Chen et al., 2018). Cleaned reads were then mapped to the zebrafish reference genome (GRCz11)

using hisat2.1.0 (Kim et al., 2019) and mapped reads were counted with FeatureCounts from the Subread package (Liao et al., 2014) using annotation from Ensembl (Danio_rerio.GRCz11.95.gtf). Differentially expressed gene (DEG) analysis was performed using the EdgeR package (Robinson and Oshlack, 2010). Genes with false discovery rates (FDR) < 0.01 were considered significant DEGs. The EnhancedVolcano package (Blighe et al., 2018) was used to create a volcano plot with Log_2FoldChange (wildtype – mutant) values and FDR calculated with EdgeR. Differences in alternative splicing between mutant and wild type was tested using the DEXseq package (Anders et al., 2012). Adjusted p-value < 0.01 was considered as significant.

ATAC sequencing

48-hpf embryos were used for ATAC sequencing. We used the Kaestner Lab ATAC seq protocol (Ackermann and Kaestner, 2019) until library preparation, followed by sequencing using a NovaSeq6000 SP. We generated reads for three independent *banp*^{rw337} mutant samples, as well as three independent *banp*^{rw337} wild-type sibling samples. Each sample contained a pool of 3 embryo heads. A quality check of reads was performed using FastQC. Reads from each sample were adaptor trimmed and aligned using fastp and Bowtie2 to the zebrafish reference genome (GRCz11) (Langmead and Salzberg, 2012) respectively. For quality control, aligned reads were filtered for low-quality reads, non-unique alignments, and PCR duplicates using samtools (Li et al., 2009; Yan et al., 2020). Moreover, alignment files were peak-called using Genrich, with removal of mitochondrial reads (Gaspar, 2019). Differences in differentially enriched peaks in wild-type and mutant embryos were identified using the DiffBind R package (Stark and Brown, 2021). The obtained peaks were annotated using the annotatePeaks tool of HOMER software (Heinz et al., 2010). The findMotifsGenome tool of HOMER (Hypergeometric Optimization of Motif EnRichment) was used to find enriched motifs in differentially expressed peaks. To compare coverage tracks across genes of interest in *banp*^{rw337} mutants and wild-type fish in RNA-seq and ATAC-seq data, distributions of mapped reads in each replicate were averaged and plotted with SparK (Kurtenbach and Harbour, 2019).

Statistics

Significance of differences between groups (wild type vs mutant) was tested using GraphPad Prism (GraphPad Software Version 9.1.2). The number of samples used per experiment is represented within figures or figure legends. Tests used to calculate statistical significance are mentioned in figure legends. All data are presented as means ± SDs. A p value of 0.05 was considered statistically significant. In the histogram, p*< 0.05, p**< 0.01, p***< 0.001, p****< 0.0001, or ns (not significant) is indicated.

Acknowledgements

We thank four former lab members, Masahiro Yamaguchi, Noriko Tonou-Fujimori, Yukihiro Yoshimura, Eri Oguri for supporting the initial phase of mapping and cloning experiments, and three technical staff members, Jeff Liner, Mamoru Fujiwara, and Tetsuya Harakuni for supporting mutant fish maintenance, immunohistochemistry, and DNA construction. We thank SQC, Research support division, Okinawa Institute of Science and Technology Graduate University for assistance in sequencing experiments. We thank Steven D. Aird for editing the manuscript.

Competing interests

The authors declare no competing or financial interests.

Author contributions

Conceptualization: SB, YT, IM; Methodology: SB, YT, IM; Software: SB, YT, IM; Validation: SB, YT, IM; Formal analysis: SB, YT, IM; Investigation: SB, YT, IM; Resources: SB, YT, IM; Data curation: SB, YT, IM; Writing - original draft: SB, IM; Writing - review & editing: SB, IM; Visualization: SB, IM; Supervision: IM; Project administration: SB, IM; Funding acquisition: IM.

Funding

This work was supported by a grant from the Okinawa Institute of Science and Technology Graduate University to IM.

Data availability

Raw RNA-seq and ATAC-seq datasets of *banp*^{rw337} mutant and wild-type siblings are available at DDBJ Sequence Read Archive (DRA012572).

References

Ackermann, A., and L. Kaestner. 2019. **UPDATED** ATAC-seq Protocol.

Anders, S., A. Reyes, and W. Huber. 2012. Detecting differential usage of exons from RNA-seq data. *Genome Research*. 22:2008-2017.

Andrews, S. 2010. FastQC: A Quality Control Tool for High Throughput Sequence Data.

Baylin, S.B., M. Esteller, M.R. Rountree, K.E. Bachman, K. Schuebel, and J.G. Herman. 2001. Aberrant patterns of DNA methylation, chromatin formation and gene expression in cancer. *Hum Mol Genet*. 10:687-692.

Berti, M., D. Cortez, and M. Lopes. 2020. The plasticity of DNA replication forks in response to clinically relevant genotoxic stress. *Nat Rev Mol Cell Bio*. 21:633-651.

Bhagat, P.N., S.H. Jadhav, S. Chattopadhyay, and K.M. Paknikar. 2018. Carbon nanospheres mediated nuclear delivery of SMAR1 protein (DNA binding domain) controls breast tumor in mice model. *Nanomedicine (Lond)*. 13:353-372.

Birot, A., L. Duret, L. Bartholin, B. Santalucia, I. Tigaud, J. Magaud, and J. Rouault. 2000. Identification and molecular analysis of BANP. *Gene*. 253:189-196.

Blackford, A.N., and S.P. Jackson. 2017. ATM, ATR, and DNA-PK: The Trinity at the Heart of the DNA Damage Response. *Molecular Cell*. 66:801-817.

Bladen, C.L., W.K. Lam, W.S. Dynan, and D.J. Kozlowski. 2005. DNA damage response and Ku80 function in the vertebrate embryo. *Nucleic Acids Res*. 33:3002-3010.

Bladen, C.L., S. Navarre, W.S. Dynan, and D.J. Kozlowski. 2007. Expression of the Ku70 subunit (XRCC6) and protection from low dose ionizing radiation during zebrafish embryogenesis. *Neurosci Lett*. 422:97-102.

Blasquez, V.C., A.O. Sperry, P.N. Cockerill, and W.T. Garrard. 1989. Protein - DNA Interactions at Chromosomal Loop Attachment Sites. *Genome*. 31:503-509.

Blighe, K., S. Rana, and M. Lewis. 2018. EnhancedVolcano: Publication-ready volcano plots with enhanced colouring and labeling.

Boije, H., R.B. MacDonald, and W.A. Harris. 2014. Reconciling competence and transcriptional hierarchies with stochasticity in retinal lineages. *Curr Opin Neurobiol*. 27:68-74.

Chattopadhyay, S., R. Kaul, A. Charest, D. Housman, and J.Z. Chen. 2000. SMAR1, a novel, alternatively spliced gene product, binds the scaffold/matrix-associated region at the T cell receptor beta locus. *Genomics*. 68:93-96.

Chaudhary, N., K.K. Nakka, P.L. Chavali, J. Bhat, S. Chatterjee, and S. Chattopadhyay. 2014. SMAR1 coordinates HDAC6-induced deacetylation of Ku70 and dictates cell fate upon irradiation. *Cell Death Dis*. 5:e1447.

Chemmannur, S.V., A.J. Badhwar, B. Mirlekar, S.K. Malonia, M. Gupta, N. Wadhwa, R. Bopanna, U. Mabalirajan, S. Majumdar, B. Ghosh, and S. Chattopadhyay. 2015. Nuclear matrix binding protein SMAR1 regulates T-cell differentiation and allergic airway disease. *Mucosal Immunol*. 8:1201-1211.

Chen, J. 2016. The Cell-Cycle Arrest and Apoptotic Functions of p53 in Tumor Initiation and Progression. *Cold Spring Harb Perspect Med*. 6:a026104.

Chen, J., S.M. Ng, C. Chang, Z. Zhang, J.C. Bourdon, D.P. Lane, and J. Peng. 2009. p53 isoform delta113p53 is a p53 target gene that antagonizes p53 apoptotic activity via BclxL activation in zebrafish. *Genes Dev*. 23:278-290.

Chen, J., H. Ruan, S.M. Ng, C. Gao, H.M. Soo, W. Wu, Z. Zhang, Z. Wen, D.P. Lane, and J. Peng. 2005. Loss of function of def selectively up-regulates Delta113p53 expression to arrest expansion growth of digestive organs in zebrafish. *Genes Dev*. 19:2900-2911.

Chen, S.F., Y.Q. Zhou, Y.R. Chen, and J. Gu. 2018. fastp: an ultra-fast all-in-one FASTQ preprocessor. *Bioinformatics*. 34:884-890.

Chen, Y.C., S. Semenova, S. Rozov, M. Sundvik, J.L. Bonkowsky, and P. Panula. 2016. A Novel Developmental Role for Dopaminergic Signaling to Specify Hypothalamic Neurotransmitter Identity. *Journal of Biological Chemistry*. 291:21880-21892.

Dowling, J.E. 2012. The Retina, An Approachable Part of the Brain. Harvard University press.

Gaspar, J.M. 2019. ATAC-seq Guidelines.

Gong, L., H. Gong, X. Pan, C. Chang, Z. Ou, S. Ye, L. Yin, L. Yang, T. Tao, Z. Zhang, C. Liu, D.P. Lane, J. Peng, and J. Chen. 2015. p53 isoform Delta113p53/Delta133p53 promotes DNA double-strand break repair to protect cell from death and senescence in response to DNA damage. *Cell Res*. 25:351-369.

Gong, L., X. Pan, G.K. Abali, J.B. Little, and Z.M. Yuan. 2020. Functional interplay between p53 and Delta 133p53 in adaptive stress response. *Cell Death and Differentiation*. 27:1618-1632.

Grand, R.S., L. Burger, C. Grawe, A.K. Michael, L. Isbel, D. Hess, L. Hoerner, V. Iesmantavicius, S. Durdu, M. Pregnolato, A.R. Krebs, S.A. Smallwood, N. Thoma, M. Vermeulen, and D. Schubeler. 2021. BANP opens chromatin and activates CpG-island-regulated genes. *Nature*.

Hart, C.M., and U.K. Laemmli. 1998. Facilitation of chromatin dynamics by SARs. *Current Opinion in Genetics & Development*. 8:519-525.

Heinz, S., C. Benner, N. Spann, E. Bertolino, Y.C. Lin, P. Laslo, J.X. Cheng, C. Murre, H. Singh, and C.K. Glass. 2010. Simple combinations of lineage-determining transcription factors prime cis-regulatory elements required for macrophage and B cell identities. *Mol Cell*. 38:576-589.

Hu, M., and S.S. Easter. 1999. Retinal neurogenesis: The formation of the initial central patch of postmitotic cells. *Dev Biol*. 207:309-321.

Hu, Z., J. Holzschuh, and W. Driever. 2015. Loss of DDB1 Leads to Transcriptional p53 Pathway Activation in Proliferating Cells, Cell Cycle Deregulation, and Apoptosis in Zebrafish Embryos. *PLoS One*. 10:e0134299.

Hung, C.Y., B. Volkmar, J.D. Baker, J.W. Bauer, E. Gussoni, S. Hainzl, A. Klausegger, J. Lorenzo, I. Mihalek, O. Rittinger, M. Tekin, J.E. Dallman, and O.A. Bodamer. 2017. A defect in the inner kinetochore protein CENPT causes a new syndrome of severe growth failure. *PLoS One*. 12:e0189324.

Imai, F., A. Yoshizawa, N. Fujimori-Tonou, K. Kawakami, and I. Masai. 2010. The ubiquitin proteasome system is required for cell proliferation of the lens

epithelium and for differentiation of lens fiber cells in zebrafish. *Development*. 137:3257-3268.

Jalota, A., K. Singh, L. Pavithra, R. Kaul-Ghanekar, S. Jameel, and S. Chattopadhyay. 2005. Tumor suppressor SMAR1 activates and stabilizes p53 through its arginine-serine-rich motif. *J Biol Chem*. 280:16019-16029.

Joruiz, S.M., J.A. Beck, I. Horikawa, and C.C. Harris. 2020. The Delta 133p53 Isoforms, Tuners of the p53 Pathway. *Cancers*. 12.

Joruiz, S.M., and J.C. Bourdon. 2016. p53 Isoforms: Key Regulators of the Cell Fate Decision. *Cold Spring Harb Perspect Med*. 6.

Jusuf, P.R., and W.A. Harris. 2009. Ptf1a is expressed transiently in all types of amacrine cells in the embryonic zebrafish retina. *Neural Dev*. 4.

Kaul, R., S. Mukherjee, F. Ahmed, M.K. Bhat, R. Chhipa, S. Galande, and S. Chattopadhyay. 2003. Direct interaction with and activation of p53 by SMAR1 retards cell-cycle progression at G2/M phase and delays tumor growth in mice. *Int J Cancer*. 103:606-615.

Kaul-Ghanekar, R., S. Majumdar, A. Jalota, N. Gulati, N. Dubey, B. Saha, and S. Chattopadhyay. 2005. Abnormal V(D)J recombination of T cell receptor beta locus in SMAR1 transgenic mice. *J Biol Chem*. 280:9450-9459.

Kim, D., J.M. Paggi, C. Park, C. Bennett, and S.L. Salzberg. 2019. Graph-based genome alignment and genotyping with HISAT2 and HISAT-genotype. *Nat Biotechnol*. 37:907-+.

Kurtenbach, S., and J.W. Harbour. 2019. SparK: A Publication-quality NGS Visualization Tool. *bioRxiv*.

Langheinrich, U., E. Hennen, G. Stott, and G. Vacun. 2002. Zebrafish as a model organism for the identification and characterization of drugs and genes affecting p53 signaling. *Curr Biol*. 12:2023-2028.

Langmead, B., and S.L. Salzberg. 2012. Fast gapped-read alignment with Bowtie 2. *Nat Methods*. 9:357-U354.

Larison, K.D., and R. Bremiller. 1990. Early Onset of Phenotype and Cell Patterning in the Embryonic Zebrafish Retina. *Development*. 109:567-&.

Li, H., B. Handsaker, A. Wysoker, T. Fennell, J. Ruan, N. Homer, G. Marth, G. Abecasis, R. Durbin, and G.P.D. Proc. 2009. The Sequence Alignment/Map format and SAMtools. *Bioinformatics*. 25:2078-2079.

Li, Z., M. Hu, M.J. Ochocinska, N.M. Joseph, and S.S. Easter, Jr. 2000. Modulation of cell proliferation in the embryonic retina of zebrafish (Danio rerio). *Dev Dyn*. 219:391-401.

Liao, Y., G.K. Smyth, and W. Shi. 2014. featureCounts: an efficient general purpose program for assigning sequence reads to genomic features. *Bioinformatics*. 30:923-930.

Liu, H.C., F. Ma, Y. Shen, Y.Q. Hu, and S. Pan. 2014. Overexpression of SMAR1 Enhances Radiosensitivity in Human Breast Cancer Cell Line MCF7 via Activation of p53 Signaling Pathway. *Oncol Res*. 22:293-300.

931 Liu, T.X., N.G. Howlett, M. Deng, D.M. Langenau, K. Hsu, J. Rhodes, J.P. Kanki, A.D.
932 D'Andrea, and A.T. Look. 2003. Knockdown of zebrafish Fancd2 causes
933 developmental abnormalities via p53-dependent apoptosis. *Dev Cell*. 5:903-914.
934 Macdonald, R., and S.W. Wilson. 1997. Distribution of Pax6 protein during eye
935 development suggests discrete roles in proliferative and differentiated visual
936 cells. *Dev Genes Evol*. 206:363-369.
937 Mahpour, A., B.S. Scruggs, D. Smiraglia, T. Ouchi, and I.H. Gelman. 2018. A methyl-
938 sensitive element induces bidirectional transcription in TATA-less CpG island-
939 associated promoters. *Plos One*. 13.
940 Malonia, S.K., S. Sinha, P. Lakshminarasimhan, K. Singh, A. Jalota-Badhwar, S. Rampalli,
941 R. Kaul-Ghanekar, and S. Chattopadhyay. 2011. Gene regulation by SMAR1:
942 Role in cellular homeostasis and cancer. *Biochim Biophys Acta*. 1815:1-12.
943 Masai, I., Z. Lele, M. Yamaguchi, A. Komori, A. Nakata, Y. Nishiwaki, H. Wada, H. Tanaka,
944 Y. Nojima, M. Hammerschmidt, S.W. Wilson, and H. Okamoto. 2003. N-
945 cadherin mediates retinal lamination, maintenance of forebrain compartments
946 and patterning of retinal neurites. *Development*. 130:2479-2494.
947 Masai, I., D.L. Stemple, H. Okamoto, and S.W. Wilson. 2000. Midline signals regulate
948 retinal neurogenesis in zebrafish. *Neuron*. 27:251-263.
949 Mathai, J., S.P. Mittal, A. Alam, P. Ranade, D. Mogare, S. Patel, S. Saxena, S. Ghorai, A.P.
950 Kulkarni, and S. Chattopadhyay. 2016. SMAR1 binds to T(C/G) repeat and
951 inhibits tumor progression by regulating miR-371-373 cluster. *Sci Rep*. 6:33779.
952 McCurley, A.T., and G.V. Callard. 2008. Characterization of housekeeping genes in
953 zebrafish: male-female differences and effects of tissue type, developmental
954 stage and chemical treatment. *Bmc Molecular Biology*. 9.
955 Mochizuki, T., Y.J. Luo, H.F. Tsai, A. Hagiwara, and I. Masai. 2017. Cell division and
956 cadherin-mediated adhesion regulate lens epithelial cell movement in zebrafish.
957 *Development*. 144:708-719.
958 Mochizuki, T., S. Suzuki, and I. Masai. 2014. Spatial pattern of cell geometry and cell-
959 division orientation in zebrafish lens epithelium. *Biol Open*. 3:982-994.
960 Murga, M., S. Bunting, M.F. Montana, R. Soria, F. Mulero, M. Canamero, Y. Lee, P.J.
961 McKinnon, A. Nussenzweig, and O. Fernandez-Capetillo. 2009. A mouse model
962 of ATR-Seckel shows embryonic replicative stress and accelerated aging. *Nat*
963 *Genet*. 41:891-U846.
964 Oliner, J.D., J.A. Pietenpol, S. Thiagalingam, J. Gyuris, K.W. Kinzler, and B. Vogelstein.
965 1993. Oncoprotein MDM2 conceals the activation domain of tumour
966 suppressor p53. *Nature*. 362:857-860.
967 Park, H.C., S.K. Hong, H.S. Kim, S.H. Kim, E.J. Yoon, C.H. Kim, N. Miki, and T.L. Huh. 2000.
968 Structural comparison of zebrafish elav/Hu and their differential expressions
969 during neurogenesis. *Neuroscience Letters*. 279:81-84.
970 Pauls, S., B. Geldmacher-Voss, and J.A. Campos-Ortega. 2001. A zebrafish histone
971 variant H2A.F/Z and a transgenic H2A.F/Z:GFP fusion protein for in vivo studies
972 of embryonic development. *Dev Genes Evol*. 211:603-610.

973 Pavithra, L., S. Mukherjee, K. Sreenath, S. Kar, K. Sakaguchi, S. Roy, and S.
974 Chattopadhyay. 2009. SMAR1 forms a ternary complex with p53-MDM2 and
975 negatively regulates p53-mediated transcription. *J Mol Biol*. 388:691-702.
976 Peterson, R.E., J.M. Fadool, J. McClintock, and P.J. Linser. 2001. Muller cell
977 differentiation in the zebrafish neural retina: Evidence of distinct early and late
978 stages in cell maturation. *Journal of Comparative Neurology*. 429:530-540.
979 Prigent, C., and S. Dimitrov. 2003. Phosphorylation of serine 10 in histone H3, what
980 for? *J Cell Sci*. 116:3677-3685.
981 Robinson, M.D., and A. Oshlack. 2010. A scaling normalization method for differential
982 expression analysis of RNA-seq data. *Genome Biol*. 11.
983 Rogakou, E.P., D.R. Pilch, A.H. Orr, V.S. Ivanova, and W.M. Bonner. 1998. DNA double-
984 stranded breaks induce histone H2AX phosphorylation on serine 139. *Journal of*
985 *Biological Chemistry*. 273:5858-5868.
986 Saito, S., A.A. Goodarzi, Y. Higashimoto, Y. Noda, S.P. Lees-Miller, E. Appella, and C.W.
987 Anderson. 2002. ATM mediates phosphorylation at multiple p53 sites, including
988 Ser(46), in response to ionizing radiation. *J Biol Chem*. 277:12491-12494.
989 Scheuermann, R.H., and W.T. Garrard. 1999. MARs of antigen receptor and co-
990 receptor genes. *Crit Rev Eukar Gene*. 9:295-310.
991 Seipold, S., F.C. Priller, P. Goldsmith, W.A. Harris, H. Baier, and S. Abdelilah-Seyfried.
992 2009. Non-SMC condensin I complex proteins control chromosome segregation
993 and survival of proliferating cells in the zebrafish neural retina. *BMC Dev Biol*.
994 9:40.
995 Shroff, R., A. Arbel-Eden, D. Pilch, G. Ira, W.M. Bonner, J.H. Petrini, J.E. Haber, and M.
996 Lichten. 2004. Distribution and dynamics of chromatin modification induced by
997 a defined DNA double-strand break. *Curr Biol*. 14:1703-1711.
998 Sidi, S., T. Sanda, R.D. Kennedy, A.T. Hagen, C.A. Jette, R. Hoffmans, J. Pascual, S.
999 Imamura, S. Kishi, J.F. Amatruda, J.P. Kanki, D.R. Green, A.A. D'Andrea, and A.T.
1000 Look. 2008. Chk1 suppresses a caspase-2 apoptotic response to DNA damage
1001 that bypasses p53, Bcl-2, and caspase-3. *Cell*. 133:864-877.
1002 Simossis, V.A., and J. Heringa. 2005. PRALINE: a multiple sequence alignment toolbox
1003 that integrates homology-extended and secondary structure information.
1004 *Nucleic Acids Research*. 33:W289-W294.
1005 Sinha, S., S.K. Malonia, S.P. Mittal, J. Mathai, J.K. Pal, and S. Chattopadhyay. 2012.
1006 Chromatin remodelling protein SMAR1 inhibits p53 dependent transactivation
1007 by regulating acetyl transferase p300. *Int J Biochem Cell Biol*. 44:46-52.
1008 Sinha, S., S.K. Malonia, S.P. Mittal, K. Singh, S. Kadreppa, R. Kamat, R. Mukhopadhyaya,
1009 J.K. Pal, and S. Chattopadhyay. 2010. Coordinated regulation of p53 apoptotic
1010 targets BAX and PUMA by SMAR1 through an identical MAR element. *EMBO J*.
1011 29:830-842.
1012 Sorrells, S., C. Toruno, R.A. Stewart, and C. Jette. 2013. Analysis of Apoptosis in
1013 Zebrafish Embryos by Whole-mount Immunofluorescence to Detect Activated
1014 Caspase 3. *Jove-J Vis Exp*.
1015 Stark, R., and G. Brown. 2021. DiffBind: Differential binding analysis of ChIP- Seq peak
1016 data.

Stiff, T., T.C. Tena, M. O'Driscoll, P.A. Jeggo, and M. Philipp. 2016. ATR promotes cilia signalling: links to developmental impacts. *Hum Mol Genet*. 25:1574-1587.

Taye, N., A. Alam, S. Ghorai, D.G. Chatterji, A. Parulekar, D. Mogare, S. Singh, P. Sengupta, S. Chatterjee, M.K. Bhat, M.K. Santra, P.B. Salunkhe, S.K. Finston, and S. Chattopadhyay. 2018. SMAR1 inhibits Wnt/beta-catenin signaling and prevents colorectal cancer progression. *Oncotarget*. 9:21322-21336.

Tibbetts, R.S., K.M. Brumbaugh, J.M. Williams, J.N. Sarkaria, W.A. Cliby, S.Y. Shieh, Y. Taya, C. Prives, and R.T. Abraham. 1999. A role for ATR in the DNA damage-induced phosphorylation of p53. *Genes Dev*. 13:152-157.

Tsuda, H., D.F. Callen, T. Fukutomi, Y. Nakamura, and S. Hirohashi. 1994. Allele loss on chromosome 16q24.2-qter occurs frequently in breast cancers irrespectively of differences in phenotype and extent of spread. *Cancer Res*. 54:513-517.

Wang, X., L. Gleich, Z.P. Pavelic, Y.Q. Li, N. Gale, S. Hunt, J.L. Gluckman, and P.J. Stambrook. 1999. Cervical metastases of head and neck squamous cell carcinoma correlate with loss of heterozygosity on chromosome 16q. *Int J Oncol*. 14:557-561.

Waterman, D.P., J.E. Haber, and M.B. Smolka. 2020. Checkpoint Responses to DNA Double-Strand Breaks. *Annu Rev Biochem*. 89:103-133.

Westerfield, M. 1993. The zebrafish book : a guide for the laboratory use of zebrafish (Brachydanio rerio).

Wilkins, B.J., K. Lorent, R.P. Matthews, and M. Pack. 2013. p53-Mediated Biliary Defects Caused by Knockdown of cirh1a, the Zebrafish Homolog of the Gene Responsible for North American Indian Childhood Cirrhosis. *Plos One*. 8.

Xu, Q., N. Holder, R. Patient, and S.W. Wilson. 1994. Spatially regulated expression of three receptor tyrosine kinase genes during gastrulation in the zebrafish. *Development*. 120:287-299.

Yadahalli, S., J.L. Neira, C.M. Johnson, Y.S. Tan, P.J.E. Rowling, A. Chattopadhyay, C.S. Verma, and L.S. Itzhaki. 2019. Kinetic and thermodynamic effects of phosphorylation on p53 binding to MDM2. *Sci Rep*. 9:693.

Yamaguchi, M., N. Fujimori-Tonou, Y. Yoshimura, T. Kishi, H. Okamoto, and I. Masai. 2008. Mutation of DNA primase causes extensive apoptosis of retinal neurons through the activation of DNA damage checkpoint and tumor suppressor p53. *Development*. 135:1247-1257.

Yan, F., D.R. Powell, D.J. Curtis, and N.C. Wong. 2020. From reads to insight: a hitchhiker's guide to ATAC-seq data analysis. *Genome Biol*. 21.

Zhang, Q., R. Su, C. Shan, C. Gao, and P. Wu. 2018. Non-SMC Condensin I Complex, Subunit G (NCAPG) is a Novel Mitotic Gene Required for Hepatocellular Cancer Cell Proliferation and Migration. *Oncol Res*. 26:269-276.

Figure Legends

Figure 1. Zebrafish *banp*^{rw337} mutants show mitotic cell accumulation and cell death in the developing retina.

(A) Morphology of wild-type and *rw337* mutant embryos at 4 dpf. *rw337* mutant embryos show smaller eyes compared to wild type at 4 dpf (red arrow). The black arrow shows the cloudy tectum in *rw337* mutant embryos, representing cell death. Scale bars: 100 μm.

(B) Plastic sections of wild-type and *rw337* mutant retinas during development. Higher magnification images of green squares in the left columns are shown in the right columns. Retinal neuroepithelium is normal in *rw337* mutants until 2 dpf. However, many round cells reminiscent of mitotic cells are accumulated in the apical region of *rw337* mutant retinas at 2 dpf (open green arrowheads), suggesting mitotic arrest of retinal progenitor cells. In wild-type retinas, three nuclear layers and two plexiform layers are form at 2.5 dpf. However, only RGCs appear near the lens and the outer region was occupied by pyknotic nuclei, indicating dead cells in *rw337* mutants. At 3 dpf, INL is formed, but the outer region is still occupied by pyknotic nuclei in *rw337* mutants. At 4 dpf, pyknotic nuclei are reduced in *rw337* mutants; however, ONL and OPL are absent despite the small number of photoreceptor-like columnar cells in putative INL (PR, asterisks). At 3 and 4 dpf, the CMZ is maintained in *rw337* mutants (green double asterisks).

(C) The *rw337* mutation is mapped in the genomic region flanked by two polymorphic markers, 070702B and zC93F2D, on chromosome 25. This genomic region contains four genes including *banp*.

(D) *banp* cDNA consists of 13 exons. In *rw337* mutants, T at the donor splice site of the intron between exons 4 and 5 (intron4/5) is converted to G, leading to the insertion of 52 nucleotides (red region) from intron 4/5. A new stop codon appears within this insertion.

(E) Wild-type Banp protein has a coiled-coil domain, a BEN domain and a DNA-binding domain. An NLS domain, an RS-rich domain, and MAR-binding domain are shown. A truncated protein missing BEN and DNA-binding domains is predicted in *rw337* mutants.

(F) Retinal sections of wild-type, wild-type embryos injected with Banp-5misMO and banp MO. *banp* morphant retinas have similar phenotypes to *banp*^{rw337} mutants, with increased cell death and loss of the ONL. Yellow open arrowheads show pyknotic nuclei.

(G) Retinal section of wild-type retinas, *banp*^{rw337} mutant retinas, and *banp*^{rw337} mutant retinas overexpressing Banp(wt)-EGFP and EGFP-Banp(rw337). Overexpression of Banp(wt)-EGFP inhibits cell death and recovers retinal lamination in *banp*^{rw337} mutants, whereas overexpression of EGFP-Banp(rw337) does not inhibit retinal defects in *banp*^{rw337} mutants. Yellow open arrowheads indicate pyknotic cells in *banp*^{rw337} mutant retinas and *banp*^{rw337} mutant retinas overexpressing EGFP-Banp(rw337).

Scale bars: 20 μm for (B, F, G).

RGC, retinal ganglion cell; AC, amacrine cell, BP, bipolar cell; HC, horizontal cell; PR, photoreceptor; OPL, outer plexiform layer; IPL, inner plexiform layer; INL, inner nuclear layer; CMZ, ciliary marginal zone.

Figure Supplement 1. Retinal cell differentiation in *banp*^{rw337} mutants at 4 dpf.

Figure Supplement 2. Amino acid conservation of Banp protein between zebrafish, mice and humans.

Figure Supplement 3. *banp*^{sa12976} homozygous mutants phenocopy *rw337* mutants.

Figure Supplement 4. Confirmation of specificity of banp MO and nuclear localization of zebrafish Banp protein.

Figure Supplement 5. Spatio-temporal pattern of zebrafish *banp* mRNA expression.

Figure 2. *banp* mutant retinas show mitotic arrest and apoptosis.

(A) TUNEL of wild-type (upper) and *banp*^{rw337} mutant (lower) retinas. In *banp*^{rw337} mutants, apoptotic cells start to be observed in the neural retinas at 53 hpf, and increase in the apical region of retinas (white arrowheads) and at the interface between the CMZ and the central retina (yellow open arrowheads) at 77 and 101 hpf.

(B) Labeling of wild-type (upper) and *banp*^{rw337} mutant (lower) retinas with anti-pH3 antibody. Mitotic cells are accumulated at the apical surface of *banp*^{rw337} mutant

retinas at 53 hpf (white open arrowheads) and restricted in the apical region of the CMZ (yellow open arrow) at 77 and 101 hpf.

(C) The number of TUNEL-positive cells per retina. Apoptosis is significantly increased in *banp*^{rw337} mutants after 53 hpf. Unpaired t-test, two-tailed, Mean ± SD. [n=3, p**< 0.01]

(D) The number of pH3-positive cells per retina. The number of mitotic cells is significantly increased in *banp*^{rw337} mutants at 53 hpf. The number is decreased, but still significantly higher in *banp*^{rw337} mutants than in wild-type siblings after 77 hpf. Unpaired t-test, two-tailed, Mean ± SD. [n=3, p**< 0.01]

(E) Schematic diagram of wild-type retinas from 48 to 77 hpf. Neuronal differentiation proceeds from the central to the peripheral retina. At 48 hpf, the proliferating area is gradually restricted in the CMZ; however, there are still retinal progenitor cells that proliferate in the central retina. Daughter cells start to exit from the cell cycle to produce differentiated neurons (light green color). At 77 hpf, most progenitor cells exit from the cell cycle, except at the CMZ. BrdU-labeled cells and pH3-positive cells are indicated in blue and green, respectively.

(F) Schematic diagram of *banp*^{rw337} mutant retinas from 48 to 77 hpf. At 48 hpf, mitotic cells are significantly accumulated at the apical surface of the neural retina and apoptosis starts in the intermediate region of the central retina. At 77 hpf, the apoptotic area is more restricted to the apical region of the retina and at the interface between the central retina and the CMZ. Mitotic cells accumulate in the apical region of the CMZ at 77 hpf. TUNEL-positive cells are indicated in magenta.

Scale bars: 20 μm for (A, B).

Source data 1. Data for Figure 2CD.

Figure Supplement 1. Apoptosis is induced in retinal progenitor cells and newly differentiating neurons in *banp*^{rw337} mutants.

Figure 3. tp53-mediated DNA damage response is activated in the absence of Banp.

(A) A volcano plot indicating gene differential expression of 48 hpf wild-type versus *banp*^{rw337} mutant embryos. Red dots show genes that were upregulated ≥2-fold in mutants, while blue dots represent genes downregulated ≥ 2-fold.

(B) Heat map of the top 15 differentially expressed genes.

(C) Relative mRNA expression levels for *bbc3*, *ccng1*, *mdm2*, *cdkn1a* in wild type and *banp*^{rw337} mutants. Quantitative RT-PCR confirmed the up-regulation of p53 pathway genes in *banp*^{rw337} mutants at 48 hpf. Unpaired t-test (two-tailed), Mean ± SD. [n=3, p*< 0.05, p**< 0.01, p***< 0.001, p**** < 0.0001].

(D) Western blotting of wild-type and *banp*^{rw337} mutants with anti-tp53 antibody. Full-length tp53 protein is stabilized in *banp*^{rw337} mutants, compared to wild type. β-actin protein is an endogenous control and used for normalization of tp53 protein level.

(E) Quantification of tp53 protein level relative to a control protein, β-actin, in wild-type and *banp*^{rw337} mutants. The tp53 protein level is significantly higher in *banp*^{rw337} mutants than in wild type at 48 hpf. Unpaired t-test (two-tailed), Mean ± SD. [n=3, p*< 0.05].

(F) Relative mRNA expression levels for *atm* and *atr* in wild type and *banp*^{rw337} mutants. Both mRNAs are significantly up-regulated in *banp*^{rw337} mutants at 48 hpf. Unpaired t-test (two-tailed) [n=3, p*< 0.05].

(G) TUNEL of wild-type and *banp*^{rw337} mutant retinas injected with STD MO and tp53 MO at 48 hpf and 72 hpf. Scale bars: 20 μm.

(H) Histogram of the number of TUNEL-positive cells per retinal section in wild-type and *banp*^{rw337} mutant retinas injected with STD MO and tp53 MO at 48 hpf and 72 hpf. Two way ANOVA, Turkey's multiple comparisons test, Mean ± SD. [n=3 for STD-MO at 48 hpf and tp53-MO at 72 hpf; n=4 for tp53-MO at 48 hpf and STD-MO at 72 hpf, p**** < 0.0001].

Source data 1. Data for Figure 3CEFH.

Source data 2. Data for Figure 3D.

Figure 4. Banp is required for the integrity of DNA replication and DNA damage repair.

(A) Quantitative RT-PCR-based validation of FL tp53 and Δ113tp53 mRNA expression at 48 hpf. Δ113tp53 mRNA expression is markedly higher in *banp*^{rw337} mutants than in wild-type siblings, whereas FL tp53 mRNA is not significantly different between mutants and wild-type siblings. Unpaired t-test (two-tailed), Mean ± SD. [n=3, p**< 0.01, ns (not significant)].

(B) ATAC-seq- and RNA-seq-based validation of chromatin accessibility (upper panel) and transcription level (bottom panel) of the genomic region covering both tp53 and Δ113tp53 transcription units. Data of wild-type and *banp*^{rw337} mutants are indicated in blue and red color, respectively. Light blue indicates overlapping level. The red box in ATAC-seq shows open chromatin in *banp*^{rw337} mutants in intron 4, signifying differential transcription of Δ113tp53 using an internal promoter.

(C) TUNEL (top), anti-pH3 antibody labeling (middle), and anti-γ-H2AX antibody labeling (bottom) of wild-type and *banp*^{rw337} mutant retinas injected with STD MO, tp53 MO, and Δ113tp53 MO. tp53 MO-mediated knockdown completely rescues apoptosis in *banp*^{rw337} mutant retinas at 48 hpf. However, Δ113tp53 MO-mediated knockdown mildly inhibits apoptosis in *banp*^{rw337} mutant retinas. Neither tp53 MO nor Δ113tp53 MO effectively rescued mitotic arrest and accumulation of γ-H2AX-positive cells (white arrowheads) in *banp*^{rw337} mutant retinas. Scale bars: 20 μm.

(D–F) Histogram of the number of TUNEL-positive cells (D), pH3-positive cells (E), and γ-H2AX-positive cells (F) per retinal section in wild-type and *banp*^{rw337} mutants injected with STD-MO, tp53 MO, and Δ113tp53 MO. Two way ANOVA with Tukey's multiple comparisons test, Mean ± SD. [n= in graph, p*< 0.05, p**< 0.01, p***< 0.001, p****< 0.0001, ns (not significant)].

(G) Possible role of Banp in tp53-mediated the DNA damage response pathway. DNA replication stress and subsequent DNA damage activate ATR and ATM, respectively, which subsequently inhibit Mdm2-mediated tp53 degradation. Stabilized tp53 mainly promotes transcription of the Δ113tp53 isoform, which activates cell-cycle arrest genes and promotes DNA damage repair. Chronic activation of tp53 activates apoptotic genes to induce apoptosis. Banp may normally suppress DNA replication stress and also promote DNA damage repair.

Source data 1. Data for Figure 4ADEF.

Figure supplement 1. DNA damage is induced in retinal progenitor cells in *banp* knockdown.

Figure 5. Banp promotes transcription of chromosome segregation regulators, *cenpt* and *ncapg*.

(A) Quantitative RT-PCR of *ncapg* expression at 48 hpf. *ncapg* mRNA expression is down-regulated in *banp*^{rw337} mutants and *banp* morphants. Unpaired t-test (two-tailed), Mean ± SD. [n=3, p**< 0.01].

(B) ATAC-seq and RNA-seq analysis of *ncapg* mRNA transcription. In *banp*^{rw337} mutants, chromatin access is reduced at the TSS of *ncapg* (ATAC-seq) and transcript expression is markedly decreased (RNA seq).

(C) Quantitative RT-PCR of *cenpt* expression at 48 hpf. *cenpt* mRNA expression is down-regulated in *banp*^{rw337} mutants and *banp* morphants. Unpaired t-test (two-tailed), Mean ± SD. [n=3, p**< 0.01].

(D) ATAC-seq and RNA-seq analysis on *cenpt* mRNA transcription. In *banp*^{rw337} mutants, chromatin access is reduced at TSS of *cenpt* (ATAC-seq) and transcript expression is markedly decreased (RNA seq).

(E) The motif enriched in genomic regions in which chromatin accessibility is reduced in *banp*^{rw337} mutants. This sequence shows a high similarity to the Banp motif.

(F) A schematic diagram representing the flow of RNA-sequencing combined with ATAC-sequencing to find candidates for zebrafish Banp direct target genes. HOMER was used to scan for Banp motifs in downregulated candidate genes, from RNA- and ATAC-sequencing in *banp*^{rw337} mutants. RNA sequencing yielded 31 candidates, whereas ATAC sequencing yielded 72, with 26 target genes consistent in both. These 26 candidate genes are the most likely to be target genes of Banp.

(G) STRING interactome analysis showing the interaction of Banp motif-containing genes downregulated in RNA sequencing. Black arrows specify genes related to cell-cycle regulation.

(H) Banp target candidate genes related to cell-cycle regulation. Gene ontology (GO) analysis was applied to 31 Banp motif-containing genes downregulated in RNA sequencing. 26% of these genes are engaged in the cell-cycle regulation. Others participate in a variety of non-categorized pathways.

(I) Banp motif upstream to the 5'-UTR of *ncapg*.

(J) Banp motif upstream to the 5'-UTR of *cenpt*.

Source data 1. Data for Figure 5AC.

Figure supplement 1. Motifs enriched in the closed and open chromatin area in *banp*^{rw337} mutants.

Figure 6. Banp is required for chromosomal segregation during mitosis.

(A) Time-lapse images of mitosis of retinal progenitor cells injected with banp 5misMO (upper) and banp MO (lower) at 2 dpf using *Tg [h2afv: GFP; EF1α: mCherry-zGem]* transgenic zebrafish. In retinas injected with banp 5misMO, mitosis proceeds sequentially from prophase (t=5~10 min), metaphase (t=16 min), anaphase (t=21 min), and telophase (t=24 min). On the other hand, in *banp* morphant retinas, the duration of mitosis from prophase to telophase was 67 min, significantly longer than that of the control MO (24 min). Furthermore, a prophase-like chromosome arrangement appeared abnormally (t=59) after several metaphase-like alignments (t=36 and 46), followed by anaphase (t=64) and telophase. Scale bar: 5μm.

(B) Violin plot of the duration of mitosis from prophase to telophase in retinas injected with banp 5misMO and banp MO. Mitosis in *banp* morphants is significantly longer than that of banp 5misMO injected embryos. Mann Whitney test, Mean ± SD. [n=3, p****< 0.0001]

(C) Confocal images of metaphase cells in zebrafish retinas at 48 hpf. The mitotic spindle is labeled with anti-α-tubulin antibody, whereas metaphase chromosomes are labeled with anti-pH3 antibody. The mitotic spindle is correctly attached to metaphase chromosomes in wild-type retinal cells (left panel). On the other hand, mitotic cells in *banp*^{rw337} mutants exhibit inefficient mitotic spindle attachment and poorly orientated metaphase chromosomes (right panels). Dotted circles indicate the outline of metaphase cells. Scale bar: 2μm.

(D) Percentage of cells with normal and abnormal spindle attachment in wild-type and *banp*^{rw337} mutant embryos. Two way ANOVA with Šídák's multiple comparisons test, Mean ± SD. [n=3, p****< 0.0001].

Source data 1. Data for Figure 6BD.

Figure 7. A possible model of Banp functions in DNA damage repair and chromosome segregation during mitosis.

Our study reveals two novel roles of Banp in cell-cycle regulation of retinal progenitor cells. First, Banp suppresses DNA replication stress and promotes DNA damage repair.

In the absence of Banp, a DNA replication stress sensor, ATR, is activated, leading to accumulation of DNA double-strand breaks, which activate ATM and the tp53-mediated DNA damage response pathway. tp53 activates the apoptotic pathway and promotes transcription of Δ113tp53, both of which promote cell-cycle arrest and DNA repair. Second, Banp is required for chromosome segregation during mitosis by promoting transcription of two mitotic regulators, *cenpt* and *ncapg*. Since a Banp motif is found near the TSSs of these genes, it is likely that *cenpt* and *ncapg* are direct targets of Banp.

Supplementary Figure Legends

Figure 1-figure supplement 1. Retinal cell differentiation in *banp*^{rw337} mutants at 4 dpf.

(A, B) ath5:EGFP expression in wild-type (A) and *rw337* mutant (B) retinas at 4 dpf. ath5:EGFP is strongly expressed in RGCs and weakly expressed in amacrine cells and photoreceptor precursors. In *rw337* mutants, ath5:EGFP expression in RGCs, amacrine cells and photoreceptor precursors is detected.

(C, D) Wild-type (C) and *rw337* mutant (D) retinas labeled with anti-Pax6 antibody at 4 dpf. Pax6 is strongly expressed in amacrine cells and weakly expressed in RGCs. In *rw337* mutants, amacrine cells seem to be decreased in number.

(E, F) Wild-type (E) and *rw337* mutant (F) retinas labeled with anti-Prox1 antibody at 4 dpf. Prox1is expressed in bipolar cells and horizontal cells. In *rw337* mutants, both bipolar-like round nuclei and horizontal-like flat nuclei are observed, but horizontal-like cells are very few.

(G, H) Wild-type (G) and *rw337* mutant (H) retinas labeled with zpr1 antibody at 4 dpf. zpr1 antibody labels double-cone-type photoreceptors in zebrafish. In *rw337* mutants, only a small cluster of zpr1-positive cells is observed in the ventro-nasal retina, suggesting that a majority of photoreceptors fail to differentiate in *rw337* mutants.

(I, J) Wild-type (I) and *rw337* mutant (J) retinas labeled with anti-GS antibody at 4 dpf. Anti-GS antibody labels Müller cells. In *rw337* mutants, Müller cells are decreased in number.

(K, L) Wild-type (K) and *rw337* mutant (L) retinas labeled with anti-PCNA antibody at 4 dpf. Anti-PCNA antibody labels retinal progenitor cells in the CMZ at 4 dpf. In *rw337* mutants, retinal progenitor cells are maintained in the CMZ.

(M, N) Phalloidin labeling of wild-type (M) and *rw337* mutant (N) retinas. Phalloidin visualizes retinal synaptic layers, the IPL and OPL. In *rw337* mutants, the IPL is detected, but not fully formed on the ventral side. Furthermore, there is no OPL, which is consistent with the lack of photoreceptors in *rw337* mutants. Scale bars: 20μm.

RGC, retinal ganglion cell, AC, amacrine cell; BP, bipolar cell; HC, horizontal cell; PR, photoreceptor; MG, Müller cell; RPC, retinal progenitor cell; OPL, outer plexiform layer; IPL, inner plexiform layer.

Figure 1-figure supplement 2. Amino acid conservation of Banp protein between zebrafish, mice and humans.

Alignment of Banp protein of humans (upper, ENSP00000376902), mice (middle, ENSMUSP00000026) and zebrafish (bottom, ENSDARP00000023) using a multiple sequence alignment program, PRALINE (Simossis and Heringa, 2005). Amino acid conservation is indicated by scoring and color coding from the least conserved (0, blue) to the most conserved (10, red). The BEN domain is indicated.

Figure 1-figure supplement 3. *banp*^{sa12976} homozygous mutants phenocopy *rw337* mutants.

(A) Another *banp* mutant allele, *sa12976*, carries a nonsense mutation in exon 4.

(B) Comparison of phenotypes between *banp* mutant alleles. *sa12976* homozygous *banp* mutant alleles and trans-heterozygous *rw337/sa12976* mutants show similar phenotypes to *rw337*: small eyes (left, red arrowheads) and retinal phenotypes: apoptosis and no ONL (right, open red arrowheads). Scale bars: 100 μm (left panel). Scale bars: 20 μm (right panel).

Figure 1-figure supplement 4. Confirmation of specificity of banp MO and nuclear localization of zebrafish Banp protein.

(A) Experimental design to confirm the specificity of banp MO and banp 5misMO (control MO). Co-injection of MO and RNA encoding Banp(wt)-EGFP to one-cell-stage eggs enables us to examine EGFP expression in gastrula stage-embryos at 6 hpf.

(B) banp MO effectively inhibits translation of Banp(wt)-EGFP protein in zebrafish embryos at 6 hpf and the retina at 24 hpf. On the other hand, banp 5misMO did not inhibit the translation of Banp(wt)-EGFP protein, suggesting that banp MO specifically inhibits Banp protein translation. Yellow dotted line indicates blastoderm cells covering yolk, in which GFP fluorescence was detected only in 5mismatch morphant embryos. Scale bars: 20μm.

(C) Time-lapse confocal scanning of mitosis of *Tg[EF1α:mCherry-CAAX]* transgenic wild-type retinal cells expressing Banp(wt)-EGFP. EGFP fluorescence is indicated in green, whereas mCherry-CAAX fluorescence labels plasma membrane and is indicated in magenta. White arrowheads indicate time-lapse change of a retinal progenitor cell undergoing mitosis. Banp(wt)-EGFP is localized in the nucleus in the interphase, whereas it spreads into the whole cell region during mitosis. Scale bars: 4μm.

(D) Histogram of intensity of Banp(wt)-EGFP during cell division shown in (A). Signals decline from mitosis to cytokinesis.

(E) Expression of Banp(wt)-EGFF, EGFP-Banp(wt) and EGFP-Banp(rw337) in zebrafish retina at 24 hpf. Both N-terminal and C-terminal EGFP-tagged wild-type Banp show nuclear localization, indicating that nuclear localization is conserved in zebrafish Banp. However, EGFP-Banp(rw337) is unstable and not maintained, suggesting that EGFP-Banp(rw337) is degraded, probably by the nonsense mutation decay mechanism. Scale bar: 10μm.

Source data 1. Data for Figure 1-figure supplement 4D.

Figure 1-figure supplement 5. Spatio-temporal pattern of zebrafish *banp* mRNA expression.

(A) Whole-mount *in situ* hybridization of zebrafish *banp* mRNA probe. *banp* mRNA is expressed in the 4-cell stage, suggesting maternal expression. *banp* mRNA is ubiquitously expressed during development from the sphere stage until the 21-somite stage. mRNA expression is restricted in the brain including the retina at 30 hpf. At 48 hpf, mRNA is prominently expressed in the brain, fins, and notochord. At 72 hpf and later, mRNA expression appears in neuromasts of the lateral lines (red open arrowheads). br, brain; re, retina; LL, neuromasts of the lateral line; n, notochord. Scale bars: 200 μm

(B) Frontal sections of zebrafish head labeled with *banp* RNA probe at 24 hpf and 48 hpf. *banp* mRNA is expressed in the entire neural retina at 24 hpf and in the CMZ at 48 hpf, suggesting the expression of *banp* mRNA in retinal progenitor cells. OT, optic tectum; CMZ, ciliary marginal zone. Scale bars: 50 μm

(C) Whole-mount *in situ* hybridization of *banp* mRNA expression in wild-type and *banp*^{rw337} mutant embryos at 72 hpf. *banp* mRNA expression is absent in *banp*^{rw337} mutants, suggesting non-sense mutation decay of mRNA. Scale bars: 200 μm

Figure 2-figure supplement 1. Apoptosis is induced in retinal progenitor cells and newly differentiating neurons in *banp*^{rw337} mutants.

(A) BrdU labeling of wild-type and *banp*^{rw337} mutant retinas at 48 hpf.

(B) ath5:EGFP expression of wild-type and *banp*^{rw337} mutant retinas at 48 hpf.

(C) Percentage of BrdU-positive area or ath5:EGFP-positive area relative to the total retinal area. There is no significant difference in BrdU-positive area between wild-type and *banp*^{rw337} mutant retinas. The fraction of ath5:EGFP-positive area is slightly, but significantly reduced in *banp*^{rw337} mutants compared with wild-type siblings. Unpaired t test (two tailed), Mean ± SD. [n=6, p*< 0.05, ns (not significant)].

(D) Labeling of wild-type and *banp*^{rw337} mutant retinas with anti-activated caspase 3 antibody at 48 hpf.

(E) Labeling of wild-type and *banp*^{rw337} mutant retinas with anti-pH3 antibody at 48 hpf.

(F) The number of caspase 3-positive or pH3-positive cells per section of retina. The number of caspase 3-positive cells and pH3-positive cells is significantly higher in *banp*^{rw337} mutants than in wild-type siblings. Unpaired t-test (two tailed), Mean ± SD. [n= 3, p*< 0.05, p**< 0.01].

(G) The relative position of caspase 3-positive cells or pH3-positive cells along the apico-basal axis of the neural retina: Positional value from 0 to 1 corresponds to the range from apical to basal position, respectively. In wild-type retinas (upper panel), pH3-positive cells are located in the apical region of the neural retina (peak of positional value is 0.2), whereas only one caspase 3-positive cell is located in the intermediate position of the neural retina (peak of positional value is 0.4). On the other hand, in *banp*^{rw337} mutant retina, pH3-positive cells are located in the apical region of the neural retina (peak of positional value is 0.1), whereas caspase3-positive cells are increased in number and most of them are located in the intermediate zone (peak of positional value is 0.3). Although pH3- and caspase3-positive positional ranges are slightly overlapped in *banp*^{rw337} mutant retinas, these

data suggest that apoptosis occurs in S phase of retinal progenitor cells or newly differentiating neurons migrating toward the basal region in *banp*^{rw337} mutants.

(H) Double labeling of wild-type and *banp*^{rw337} mutant retinas with ath5:EGFP transgene and anti-caspase 3 antibody.

(I) Percentage of ath5:EGFP-positive area relative to the total retinal area (left) and percentage of ath5:EGFP- and caspase 3-double positive cells relative to the total number of caspase 3-positive cells (right). Mann Whitney test, Mean ± SD. [n=7, p**< 0.01].

(J) Double labeling of wild-type and *banp*^{rw337} mutant retinas with anti-HuC/D antibody and anti-caspase 3 antibody.

(K) Percentage of HuC/D-positive area relative to the total retinal area (left) and percentage of HuC/D- and caspase 3-double positive cells relative to the total number of caspase 3-positive cells (right). Mann Whitney test, Mean ± SD. [n=7 for wild-type, n=6 for *banp*^{rw337} mutants, p*< 0.05].

(L) A possible model on how apoptosis is induced during retinal progenitor cell proliferation and retinal neurogenesis in *banp*^{rw337} mutants.

Scale bar: 20μm for (A, B, D, E, H, J)

Source data 1. Data for Figure 2-figure supplement 1CFGIK

Figure 4-figure supplement 1. DNA damage is induced in retinal progenitor cells in *banp* knockdown.

(A) Labeling of 48 hpf wild-type retinas injected with STD MO and banp MO with anti-γ-H2AX antibody. γ-H2AX-positive cells are increased in *banp* morphant retinas. Scale bars: 20μm.

(B) The number of γ-H2AX-positive cells in 48 hpf wild-type retinas injected with STD MO and banp MO. The number of γ-H2AX-positive cells is significantly higher in *banp* morphant retinas than in wild-type retinas injected with STD MO. Mann Whitney test, Mean ± SD. [n=5, p**< 0.01].

(C) Labeling of 48 hpf wild-type and *banp*^{rw337} mutant retinas with anti-BrdU antibody (red), anti-γ-H2AX antibody (blue), and ath5:EGFP transgene (green). Two independent *banp*^{rw337} mutant retinas are shown. Scale bars: 20 μm.

(D) The fraction of γ-H2AX-positive cells in the total retinal area in wild-type and *banp*^{rw337} mutants. Mann Whitney test, Mean ± SD. [n=6, p <**0.01].

(E) Double labeling of retinal CMZ in *banp*^{rw337} mutants with anti-BrdU antibody (red), anti-γ-H2AX antibody (blue). Higher magnification images of square in *banp*^{rw337} mutant retinas shown in (C).

(F) The fraction of BrdU-positive cells in the total retinal cells and γ-H2AX-positive cells in *banp*^{rw337} mutants. Mean of difference between the total retinal cells and γ-H2AX-positive cells is shown in the right side. The fraction is significantly higher in γ-H2AX-positive cells than in the total retinal cells. Paired t-test. [n=6, p <***0.001]. Correlation plot (F') indicates significantly effective pairing [p< *0.05].

(G) Double labeling of retinal CMZ in *banp*^{rw337} mutants with ath5:EGFP transgene (green), anti-γ-H2AX antibody (blue). Higher magnification images of square in *banp*^{rw337} mutant retinas shown in (C).

(H) The fraction of ath5:EGFP-positive cells in the total retinal cells and γ-H2AX-positive cells in *banp*^{rw337} mutants. Mean of difference between the total retinal cells and γ-H2AX-positive cells is shown in the right side. There is no significant difference between the total retinal cells and γ-H2AX-positive cells. Paired t-test. [n=6, ns]. Correlation plot (H') indicates no significant pairing. [ns].

(I) Labeling of 48 hpf wild-type and *banp*^{rw337} mutant retinas with anti-pH3 antibody (magenta), anti-γ-H2AX antibody (green). Top and bottom right-side panels of *banp*^{rw337} mutant retinas indicate original fluorescent images and their Imaris surface-rendered images, respectively. Scale bars: 20 μm.

(J) The fraction of pH3-positive cells in the total retinal cells and γ-H2AX-positive cells in *banp*^{rw337} mutants. Mean of difference between the total retinal cells and γ-H2AX-positive cells is shown in the right side. There is no significant difference between the total retinal cells and γ-H2AX-positive cells. Paired t-test [n=10, ns]. Correlation plot (J') indicates no significant pairing. [ns].

Source data 1. Data for Figure 4-figure supplement 1BDFHJ.

Figure 5-figure supplement 1. Motifs enriched in the closed and open chromatin area in *banp*^{rw337} mutants.

(A) List of top6 motifs enriched in genomic regions of decreased (downregulated) and increased (upregulated) accessibility in *banp*^{rw337} mutants. We found that the Banp motif (TCTCGCGAGA) is the most enriched sequence in regions with reduced chromatin accessibility in *banp*^{rw337} mutants (large arrowhead).

(B, C) A putative Banp motif with a conserved CGCG element upstream of the 5' UTR of *ncapg* (B) and *cenpt* (C) in zebrafish, mice and humans.

Video File Legends

Video 1. Time-lapse movie of mitosis of wild-type retinal progenitor cells.

Tg [h2afv: GFP; EF1α: mCherry-zGem] transgenic embryos were injected with banp 5misMO and mitosis of retinal progenitor cells was scanned with confocal LSM. Mitosis proceeds sequentially from prophase (t=5~10 min), metaphase (t=16 min), anaphase (t=21 min) and telophase (t=24 min). Green indicates GFP fluorescence, representing chromatin. On the other hand, magenta indicates fluorescence from mCherry, representing S/G2/M phase cells.

Video 2. Time-lapse movie of mitosis of *banp* morphant retinal progenitor cells.

Tg [h2afv: GFP; EF1α: mCherry-zGem] transgenic embryos were injected with banp MO and mitosis of retinal progenitor cells was scanned with confocal LSM. Mitosis did not procced smoothly, and it took longer from chromosome condensation in prophase (t=15 min) to chromosome alignment at the division plane in anaphase (t=46 min). Aligned chromosomes were often dispersed during chromosome segregation by mitotic spindle (t=46~64 min). Green indicates fluorescence from GFP, representing chromatin. On the other hand, magenta indicates fluorescence from mCherry, representing S/G2/M phase cells.

Supplementary Information

Supplementary Figures

Figure 1-figure supplement 1. Retinal cell differentiation in *banp*^{rw337} mutants at 4 dpf.

Figure 1-figure supplement 2. Amino acid conservation of Banp protein between zebrafish, mice and humans.

Figure 1-figure supplement 3. *banp*^{sa12976} homozygous mutants phenocopy *rw337* mutants.

Figure 1-figure supplement 4. Confirmation of specificity of banp MO and nuclear localization of zebrafish Banp protein.

Figure 1-figure supplement 5. Spatio-temporal pattern of zebrafish *banp* mRNA expression.

Figure 2-figure supplement 1. Apoptosis is induced in retinal progenitor cells and newly differentiating neurons in *banp*^{rw337} mutants.

Figure 4-figure supplement 1. DNA damage is induced in retinal progenitor cells in *banp* knockdown.

Figure 5-figure supplement 1. Motifs enriched in the closed and open chromatin area in *banp*^{rw337} mutants.

Supplementary Table file

Supplementary Table 1.

Source data files

Figure 2-Source data 1. Data for Figure 2CD.

Figure 3-Source data 1. Data for Figure 3CEFH.

Figure 3-Source data 2. Data for Figure 3D.

Figure 4-Source data 1. Data for Figure 4ADEF.

Figure 5-Source data 1. Data for Figure 5AC.

Figure 6-Source data 1. Data for Figure 6BD.

Figure 1-figure supplement 4-Source data 1. Data for Figure 1-figure supplement 4D.

Figure 2-figure supplement 1-Source data 1. Data for Figure 2-figure supplement 1CFGIK

Figure 4-figure supplement 1-Source data 1. Data for Figure 4-figure supplement 1BDFHJ.

Video files

Video 1. Time-lapse movie of mitosis of wild-type retinal progenitor cells.

Video 2. Time-lapse movie of mitosis of *banp* morphant retinal progenitor cells.

Appendix

Key Resources Table				
Reagent type (species) or resource	**Designation**	**Source or reference**	**Identifiers**	**Additional information**
strain, strain background (Danio Rerio)	*banp*^{rw337}	This paper		
strain, strain background (Danio Rerio)	*banp*^{sa12976}	ZIRC	ZFIN: ZDB-ALT-130411-2647	
strain, strain background (Danio Rerio)	*Tg[EF1α:mCherry-zGem]*^{oki011}	PMID: 25260917	ZFIN: ZDB-ALT-150128-2	
strain, strain background (Danio Rerio)	*Tg[EF1α:mCherry-CAAX]*^{oki049}	PMID: 28196805	ZFIN: ZDB-TGCONSTRCT-181026-1	
strain, strain background (Danio Rerio)	*Tg[h2afv:GFP]*$^{kca6/kca66}$	PMID: 11819118	ZFIN: ZDB-ALT-020918-4, ZDB-ALT-020717-2	
strain, strain background (Danio	*Tg[ath5:EGFP]*^{rw021}	PMID: 15728672	ZFIN: ZDB-ALT-050627-2	
antibody	pH3 (Mouse ,monoclonal)	Cell signaling technology	6G3, 9706	1:500 (IHC)
antibody	pH3 (Rabbit, polyclonal)	Sigma-Aldrich (Merk)	06-570	1:500 (IHC)

antibody	Caspase3 (Rabbit, monoclonal)	BD Pharmingen	Clone C92-605	1:200 (IHC)
antibody	Pax6 (Rabbit, polyclonal)	Covance	PRB-278P	1:500 (IHC)
antibody	zpr1 (Mouse, monoclonal)	ZIRC, Eugene, Oregon	ZFIN: ZDB-ATB-081002-43	1:100 (IHC)
antibody	glutamine synthetase (GS) (Mouse, monoclonal)	Millipore	MAB302, clone GS-6	1:100 (IHC)
antibody	PCNA (Mouse, monoclonal)	Sigma-Aldrich	Clone PC10,P8825	1:200 (IHC)
antibody	Prox1 (Rabbit, polyclonal)	Gene Tex	GTX128354	1:500 (IHC)
antibody	Alpha tubulin (Mouse, monoclonal)	Sigma-Aldrich	T5168, clone B512	1:1000 (IHC)
antibody	γ-H2AX (Rabbit, polyclonal)	Gene Tex	GTX127342	1:500 (IHC)
antibody	BrdU (Rat, monoclonal)	abcam	Ab6326	1:200 (IHC)
antibody	HuC/D (Mouse, monoclonal)	Thermo Fisher	A-21271	1:200 (IHC)

antibody	β-actin (Mouse, monoclonal)	Sigma-Aldrich	A5441	1:5000 (western blot)
antibody	tp53 (Rabbit, polyclonal)	Gene Tex	GTX128135	1:1000 (western blot)
antibody	Secondary antibodies, horseradish peroxidase-conjugated (Mouse)	Amersham	NA931	1:5000 (western blot)
antibody	secondary antibodies, horseradish peroxidase-conjugated (Rabbit)	Amersham	NA934	1:5000 (western blot)
recombinant DNA reagent	pBluescript II SK(+) (vector)	Stratagene/Agilent Technologies		*in vitro* transcription (In situ hybridization probe synthesis)
recombinant DNA reagent	pCS2 (expression vector)	PMID: **7926732**		*in vitro* transcription (Capped mRNA synthesis)
sequence-based reagent (mutation mapping)	Polymorphic marker to link with banp mutation locus	This paper	PCR primers	70702B forward: 5'-ACTTCTTATCAGGGCTGTGC-3' 070702B reverse: 5'-TCAGTCAAGAGCAGTGAGAG-3'
sequence-based reagent (mutation mapping)	Polymorphic markers to link banp mutation locus	This paper	PCR primers	zC93F2D forward: 5'-TGGGATCTCTTTAAGTGAGTGAG-3' zC93F2D reverse:

				5'-TCCAACTATGTGGGTCAAACC-3'
sequence-based reagent (Morpholino)	banp MO	This paper	Morpholino antisense oligos	5'-CCACTAAATCTTGCTCTGACATCAT-3'
sequence-based reagent (Morpholino)	banp 5misMO	This paper	Morpholino antisense oligos	5'-CCtCaAAATgTTcCTCTcACATCAT-3'
sequence-based reagent (Morpholino)	tp53 MO	PMID: 12477391	Morpholino antisense oligos	5'-GCGCCATTGCTTTGCAAGAATTG-3'
sequence-based reagent (Morpholino)	Δ113 tp53 MO	PMID: 19204115	Morpholino antisense oligos	5'-GCAAGTTTTTGCCAGCTGACAGAAG-3'
sequence-based reagent (Morpholino)	STD MO	PMID: 30322969	Morpholino antisense oligos	5'-CCTCTTACCTCAGTTACAATTTATA-3'
sequence-based reagent (primer)	ccng1	This paper	Primers for qRT-PCR	**Forward primer**: ccctggagattgaggatcag **Reverse primer:** cacacaaaccaggtctccaa
sequence-based reagent (primer)	mdm2	PMID: 24147052	Primers for qRT-PCR	**Forward primer**: caggaggaggagaagcagtg **Reverse primer:** agggaaaagctgtccgactt

sequence-based reagent (primer)	p21(cdkn1a)	PMID: 26908596	Primers for qRT-PCR	**Forward primer**: aagcgcaaacagaccaacat **Reverse primer:** tcagctactggccggatt
sequence-based reagent (primer)	FL tp53	PMID: 27539857	Primers for qRT-PCR	**Forward primer**: tggagaggaggtcggcaaaatcaa **Reverse primer:** gactgcgggaacctgagcctaaat
sequence-based reagent (primer)	Δ113 tp53	PMID: 27539857	Primers for qRT-PCR	**Forward primer**: atatcctggcgaacatttggaggg **Reverse primer:** cctcctggtcttgtaatgtcac
sequence-based reagent (primer)	Puma (bbc3)	This paper	Primers for qRT-PCR	**Forward primer**: ctgaggaggaccccacact **Reverse primer:** tctccagttctgccagtgc
sequence-based reagent (primer)	cenpt	This paper	Primers for qRT-PCR	**Forward primer**: tcatgaggagattgtggaagatg **Reverse primer:** ggtgagctctgcgagttatt
sequence-based reagent (primer)	ncapg	This paper	Primers for qRT-PCR	**Forward primer**: ctgatgtgagggagcctattt **Reverse primer:** gagtctgtttggcctccatta

sequence-based reagent (primer)	atm	This paper	Primers for qRT-PCR	**Forward primer**: cctcaaggctgtggagaact **Reverse primer:** aggggattttctttacaccactc
sequence-based reagent (primer)	atr	This paper	Primers for qRT-PCR	**Forward primer**: aggaacccaatctgccagt **Reverse primer:** gatgtccagtgccagctctc
sequence-based reagent (primer)	ef1α	PMID: 19014500	Primers for qRT-PCR	**Forward primer**: cttctcaggctgactgtgc **Reverse primer:** ccgctagcattaccctcc
sequence-based reagent (sequencing primer)	Genotyping primers for *banp*^{sa12976}	This paper	Primers	**Forward primer**: TGTTGATATCCATCAGTCAG **Reverse primer:** GGTGTATAAATCACATGACC
sequence-based reagent (primer)	Genotyping primers for *banp*^{rw337}	This paper	Primers	**forward:** 5'-CGATGTTGATATCCATCAGTCAGGCGATC-3'; **reverse primer:** 5'-GGTGCTGGTGTATAAATCACATGACCTATGGTCCTCTT-3'.
commercial assay or kit	DIG RNA Labelling Kit	Roche	11175025910	In situ hybridization

commercial assay or kit	mMESSAGE mMACHINE™ SP6 Transcription Kit	Invitrogen	AM1340	Capped mRNA synthesis
commercial assay or kit	In Situ Cell Death Detection Kit, TMR red	Roche	12156792910	apoptosis
commercial assay or kit	ReverTra Ace® aPCR master mix with gDNA remover	Toyobo	FSQ-301	cDNA synthesis
commercial assay or kit	Luna® Universal qPCR Master Mix	NEB	M3003L	qRT-PCR
commercial assay or kit	Direct-zol RNA Miniprep Kit	ZYMO RESEARCH	R2050	RNA-sequencing
commercial assay or kit	NEBNext® Ultra™ II Directional RNA Library Prep Kit	NEB	E7760	Illumina RNA-sequencing
chemical compound, drug	Acridine orange	WALDECK (CHROMA)	1B-307	Live cell death detection
software	IMARIS	Bitplane	ver.9.1.2	http://www.bitplane.com/imaris; RRID: SCR_007370
software	Image J	NIH	Version 2.1.0/1.53c	Percentage area calculation
software	Zen	Zeiss	LSM 710	Percentage area calculation
software	GraphPad Prism	GraphPad Software	Version 9.1.2	https://www.graphpad.com/scientific-software/prism/
other	SYTOX Green	Molecular Probes	S34862	Nuclear stain 1:1000 (IHC)
other	rhodamine-conjugated	Molecular Probes	R415	Filamentous actin (F-actin) stain

	phalloidin			1: 40 (IHC)
other	Restore™ PLUS Western Blot Stripping Buffer	Thermo Scientific	46430	Remove high-affinity antibodies from membranes (western blot)

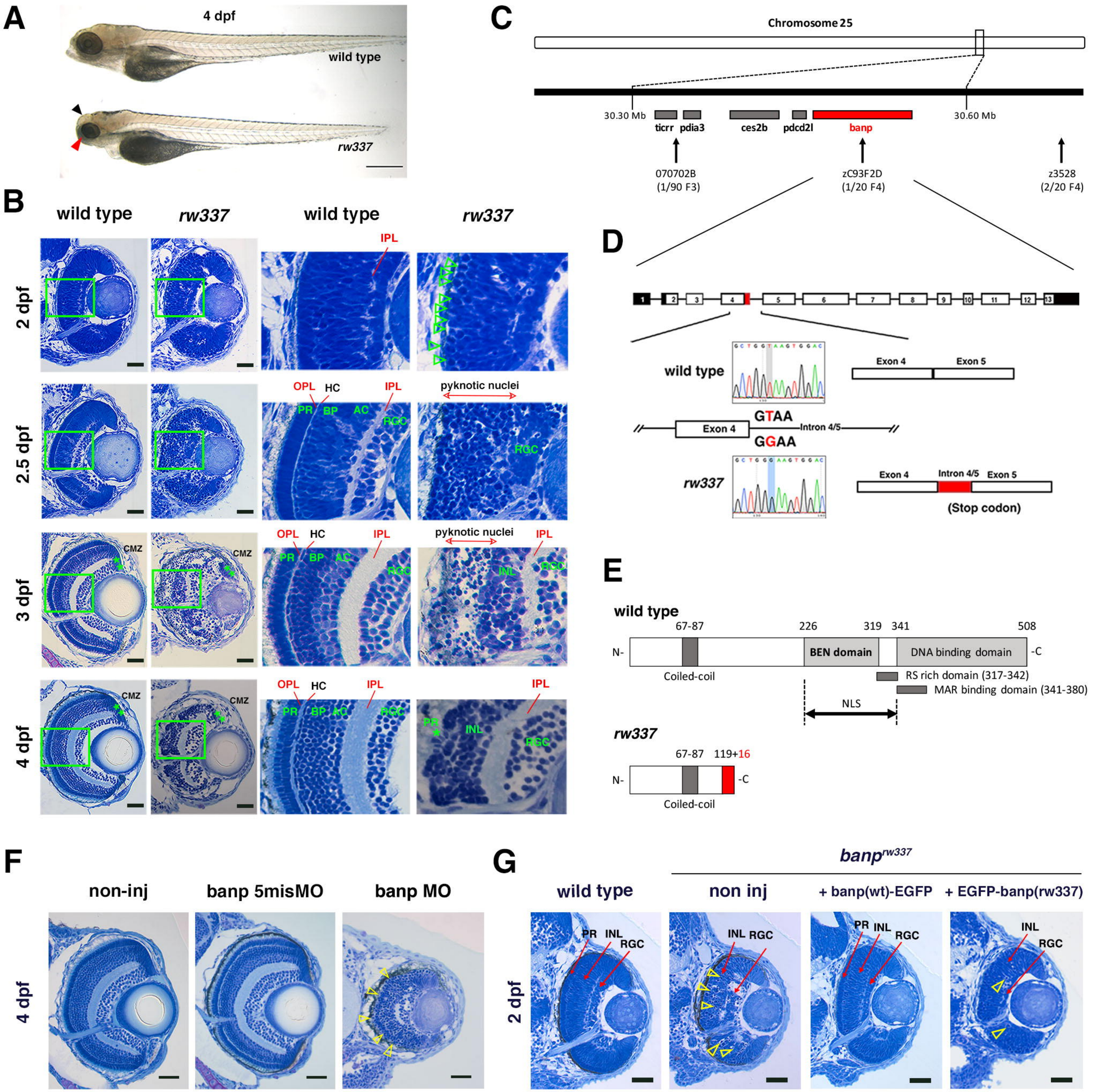
A
4 dpf
wild type
rw337
B
wild type
rw337
wild type
rw337
2 dpf
2.5 dpf
3 dpf
4 dpf
IPL
OPL
HC
PR
BP
AC
RGC
pyknotic nuclei
CMZ
INL
C
Chromosome 25
30.30 Mb
30.60 Mb
ticrr
pdia3
ces2b
pdcd2l
banp
070702B
(1/90 F3)
zC93F2D
(1/20 F4)
z3528
(2/20 F4)
D
wild type
rw337
GTAA
GGAA
Exon 4
Intron 4/5
Exon 5
(Stop codon)
E
wild type
67-87
226
319
341
508
N-
-C
BEN domain
DNA binding domain
Coiled-coil
RS rich domain (317-342)
MAR binding domain (341-380)
NLS
rw337
67-87
119+16
F
non-inj
banp 5misMO
banp MO
4 dpf
G
banp^rw337
wild type
non inj
+ banp(wt)-EGFP
+ EGFP-banp(rw337)
2 dpf

Figure 1

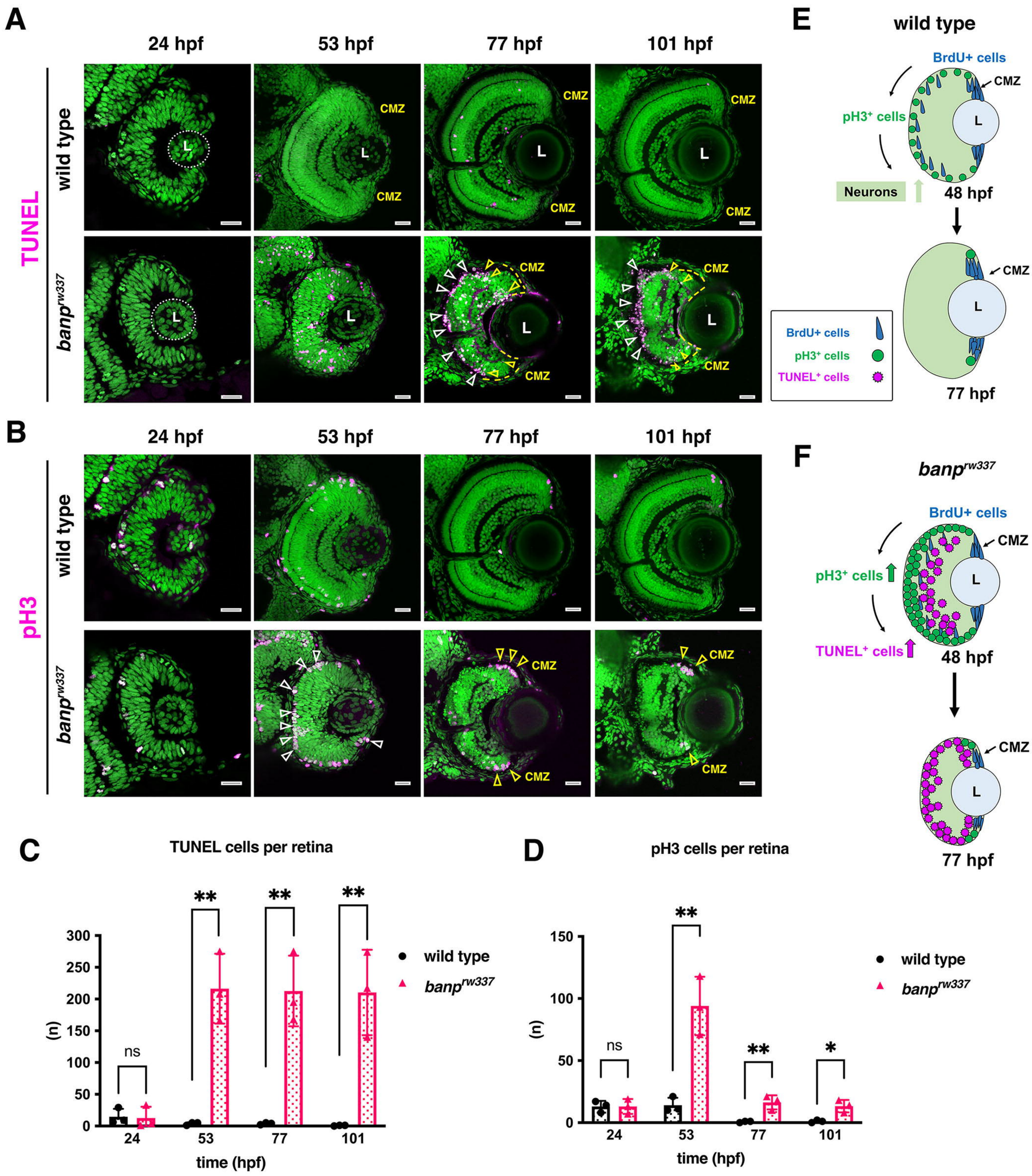
A
24 hpf
53 hpf
77 hpf
101 hpf
TUNEL
wild type
banp^rw337
L
CMZ
B
pH3
C
TUNEL cells per retina
(n)
ns
**
time (hpf)
wild type
banp^rw337
D
pH3 cells per retina
*
E
wild type
BrdU+ cells
pH3+ cells
TUNEL+ cells
Neurons
48 hpf
77 hpf
F
banp^rw337

Figure 2

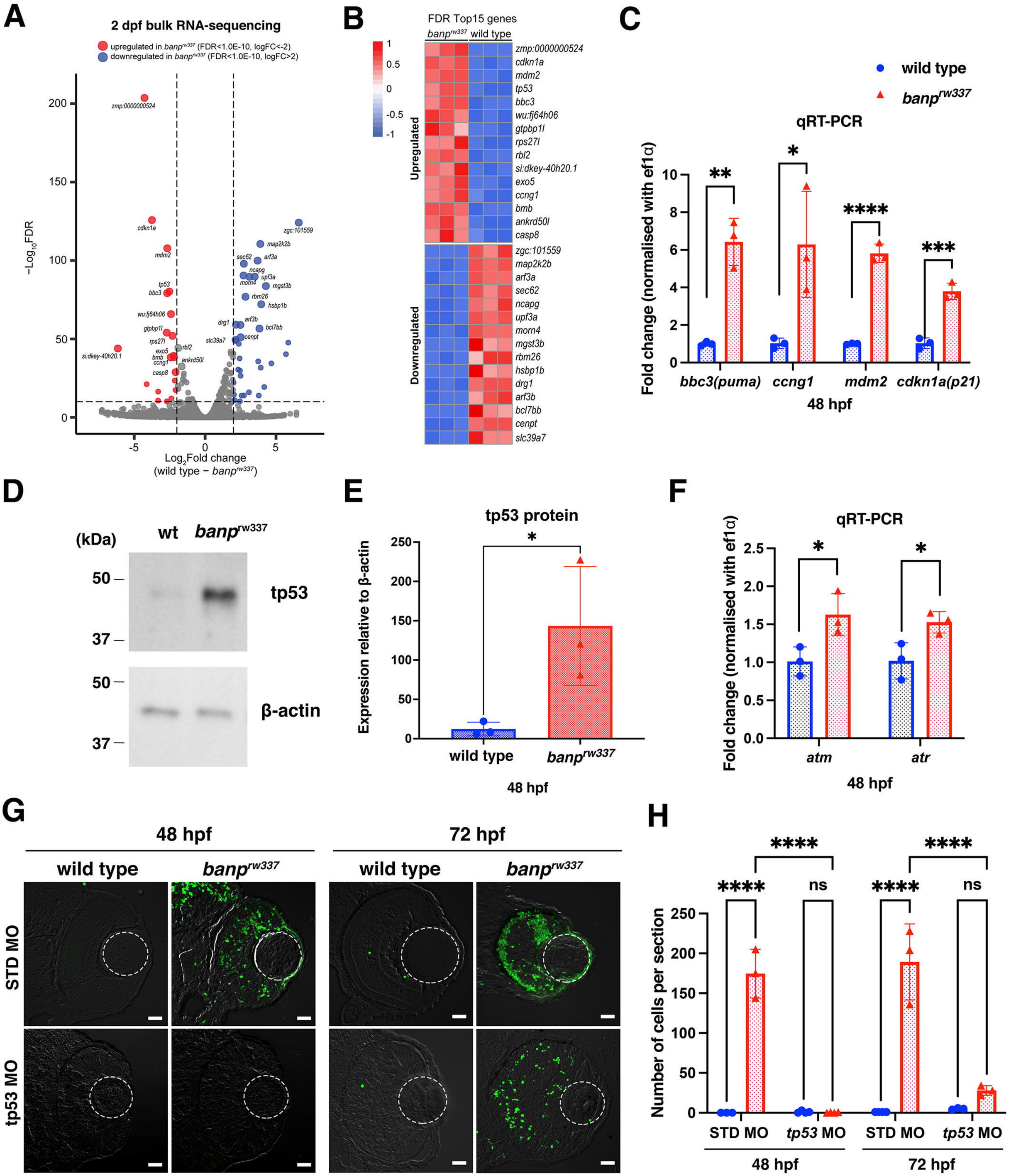
A
2 dpf bulk RNA-sequencing
upregulated in banp^rw337 (FDR<1.0E-10, logFC<-2)
downregulated in banp^rw337 (FDR<1.0E-10, logFC>2)
−Log10FDR
Log2Fold change
(wild type − banp^rw337)
zmp:0000000524
cdkn1a
mdm2
tp53
bbc3
wu:fj64h06
gtpbp1l
rps27l
si:dkey-40h20.1
exo5
bmb
ccng1
casp8
rbl2
ankrd50l
zgc:101559
map2k2b
sec62
arf3a
ncapg
upf3a
morn4
mgst3b
rbm26
hsbp1b
drg1
arf3b
bcl7bb
slc39a7
cenpt
B
FDR Top15 genes
banp^rw337
wild type
Upregulated
Downregulated
C
wild type
banp^rw337
qRT-PCR
Fold change (normalised with ef1α)
bbc3(puma)
ccng1
mdm2
cdkn1a(p21)
48 hpf
D
(kDa)
wt
banp^rw337
tp53
β-actin
E
tp53 protein
Expression relative to β-actin
wild type
banp^rw337
48 hpf
F
qRT-PCR
Fold change (normalised with ef1α)
atm
atr
48 hpf
G
48 hpf
72 hpf
wild type
banp^rw337
STD MO
tp53 MO
H
Number of cells per section
STD MO
tp53 MO
48 hpf
72 hpf
ns

Figure 3

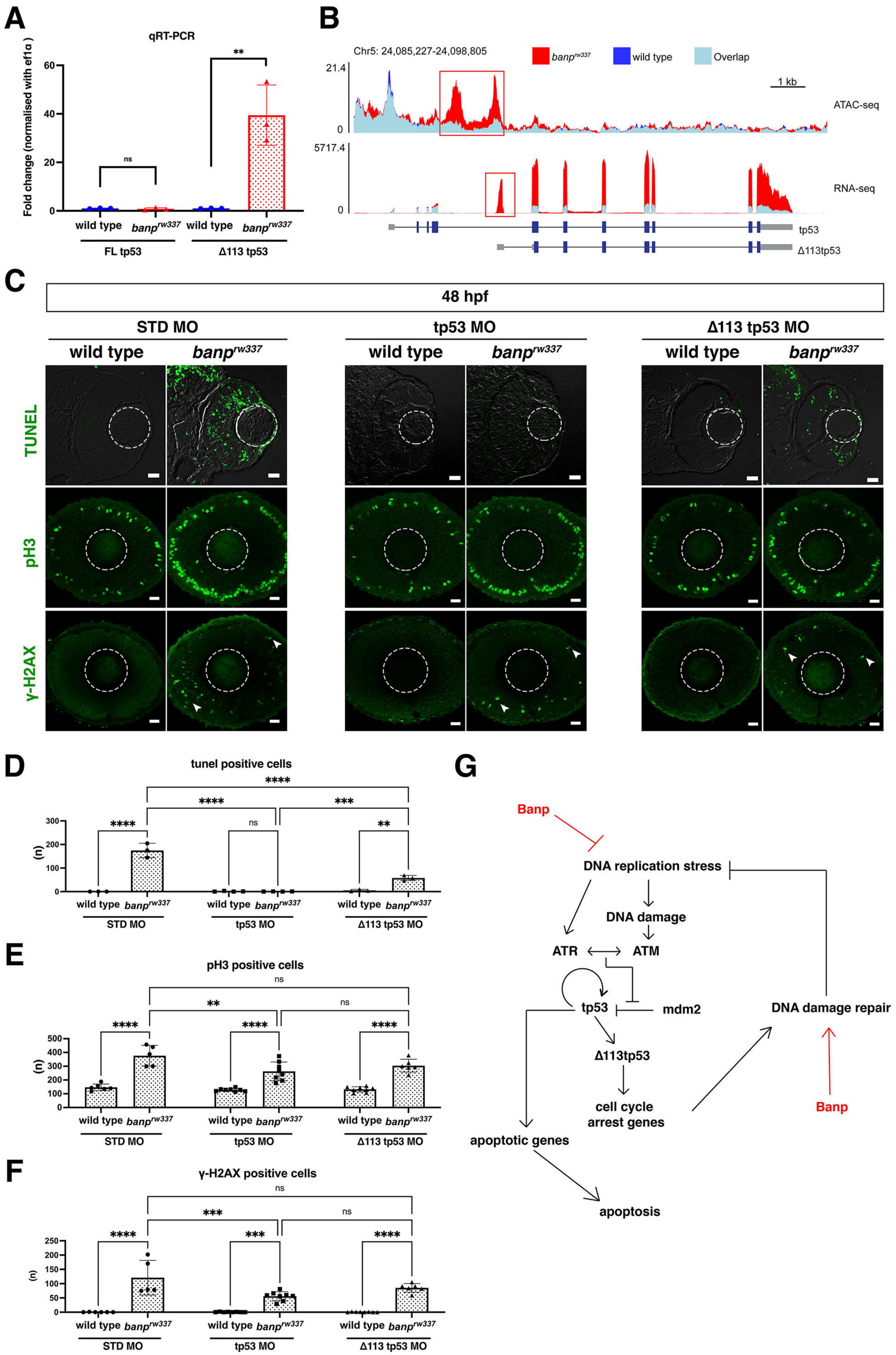
A
qRT-PCR
Fold change (normalised with ef1α)
wild type
banp rw337
FL tp53
Δ113 tp53
B
Chr5: 24,085,227-24,098,805
banp rw337
wild type
Overlap
1 kb
ATAC-seq
RNA-seq
tp53
Δ113tp53
C
48 hpf
STD MO
tp53 MO
Δ113 tp53 MO
TUNEL
pH3
γ-H2AX
D
tunel positive cells
E
pH3 positive cells
F
γ-H2AX positive cells
G
Banp
DNA replication stress
DNA damage
ATR
ATM
tp53
mdm2
DNA damage repair
Δ113tp53
cell cycle arrest genes
apoptotic genes
apoptosis

Figure 4

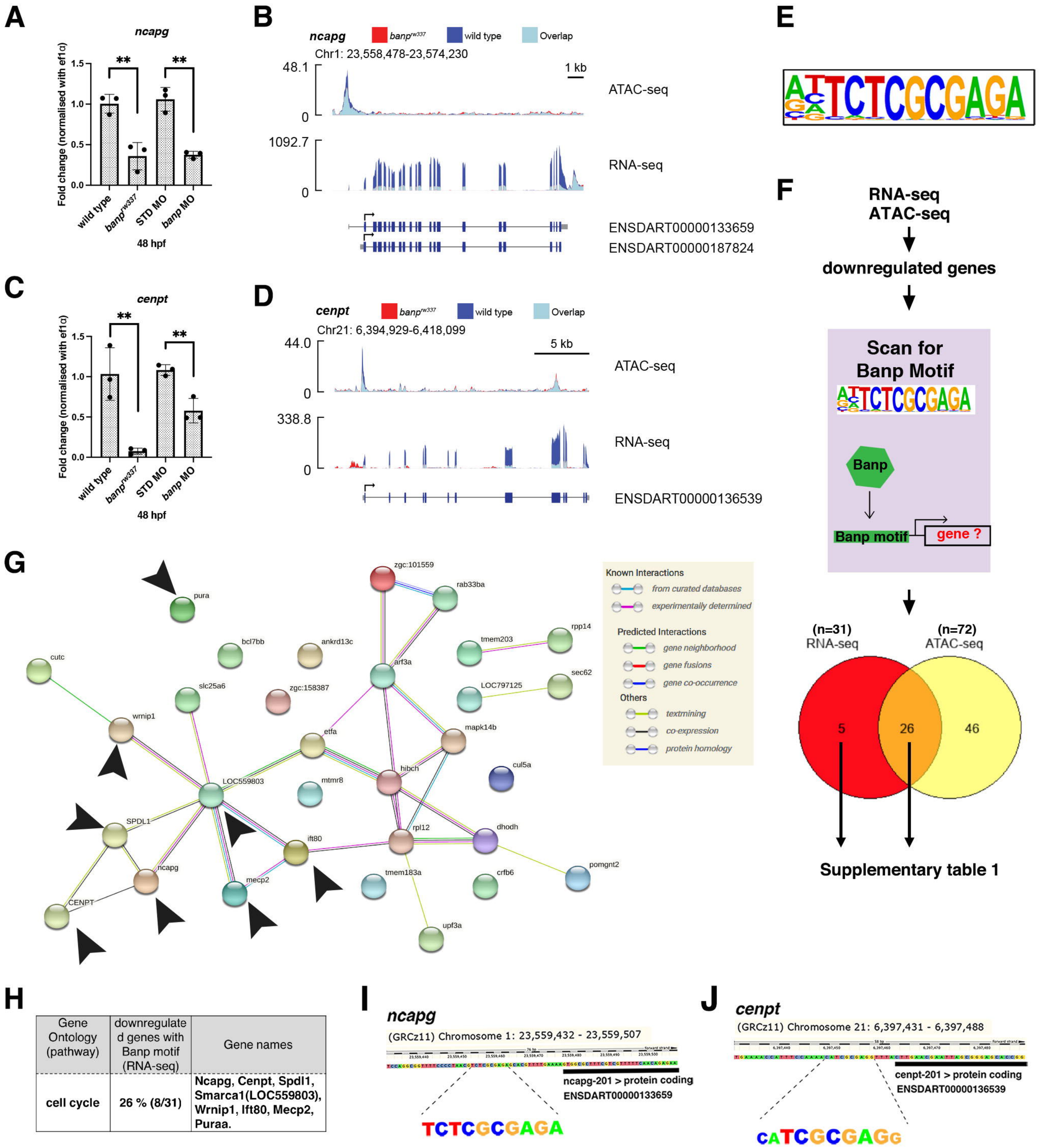

Gene Ontology (pathway)	downregulated genes with Banp motif (RNA-seq)	Gene names
cell cycle	**26 % (8/31)**	**Ncapg, Cenpt, Spdl1, Smarca1(LOC559803), Wrnip1, Ift80, Mecp2, Puraa.**

Figure 5

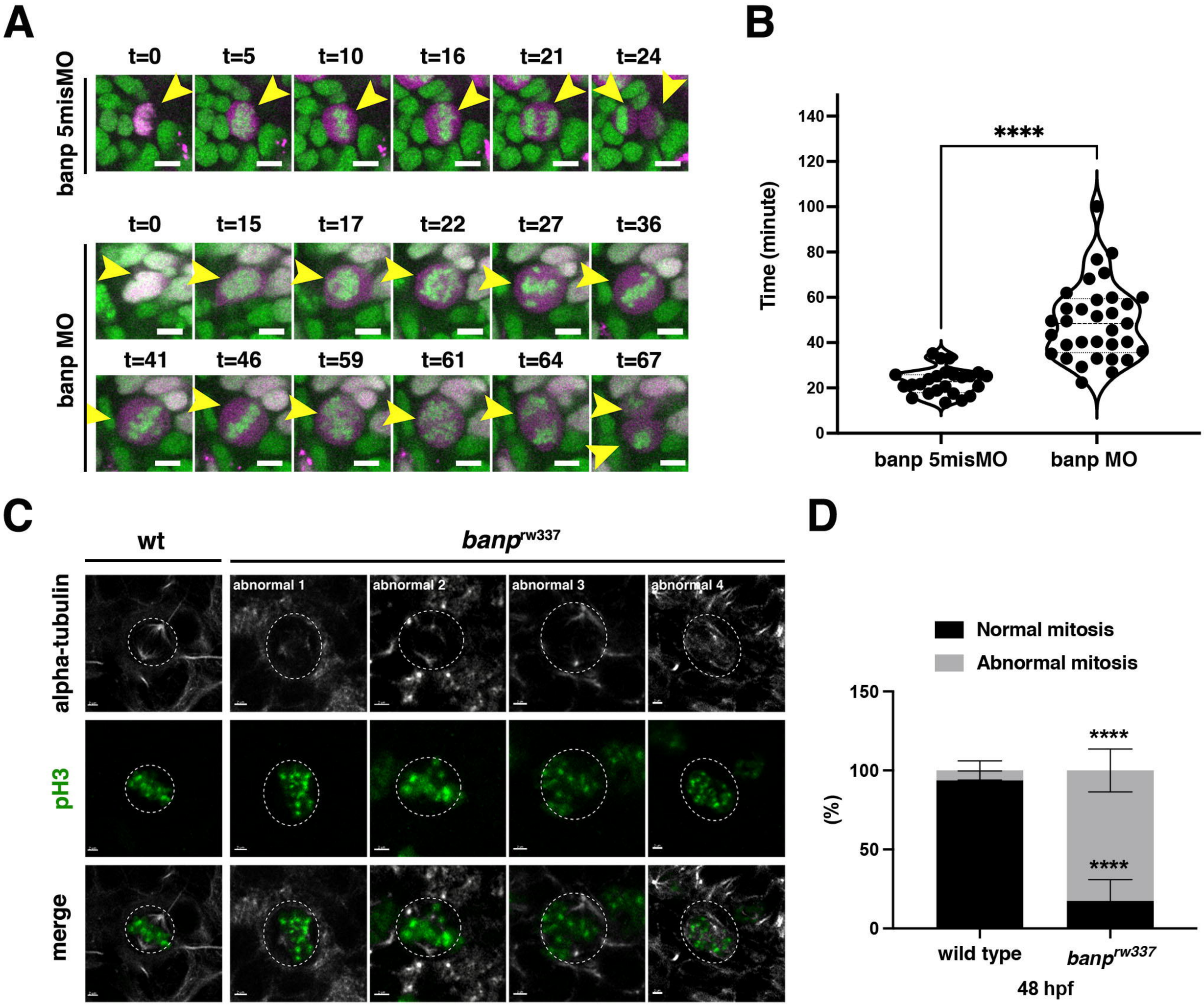
A
banp 5misMO
t=0
t=5
t=10
t=16
t=21
t=24
banp MO
t=0
t=15
t=17
t=22
t=27
t=36
t=41
t=46
t=59
t=61
t=64
t=67
B
Time (minute)
140
120
100
80
60
40
20
0
****
banp 5misMO
banp MO
C
wt
banp rw337
alpha-tubulin
pH3
merge
abnormal 1
abnormal 2
abnormal 3
abnormal 4
D
Normal mitosis
Abnormal mitosis
150
100
50
0
(%)
****
****
wild type
banp rw337
48 hpf

Figure 6

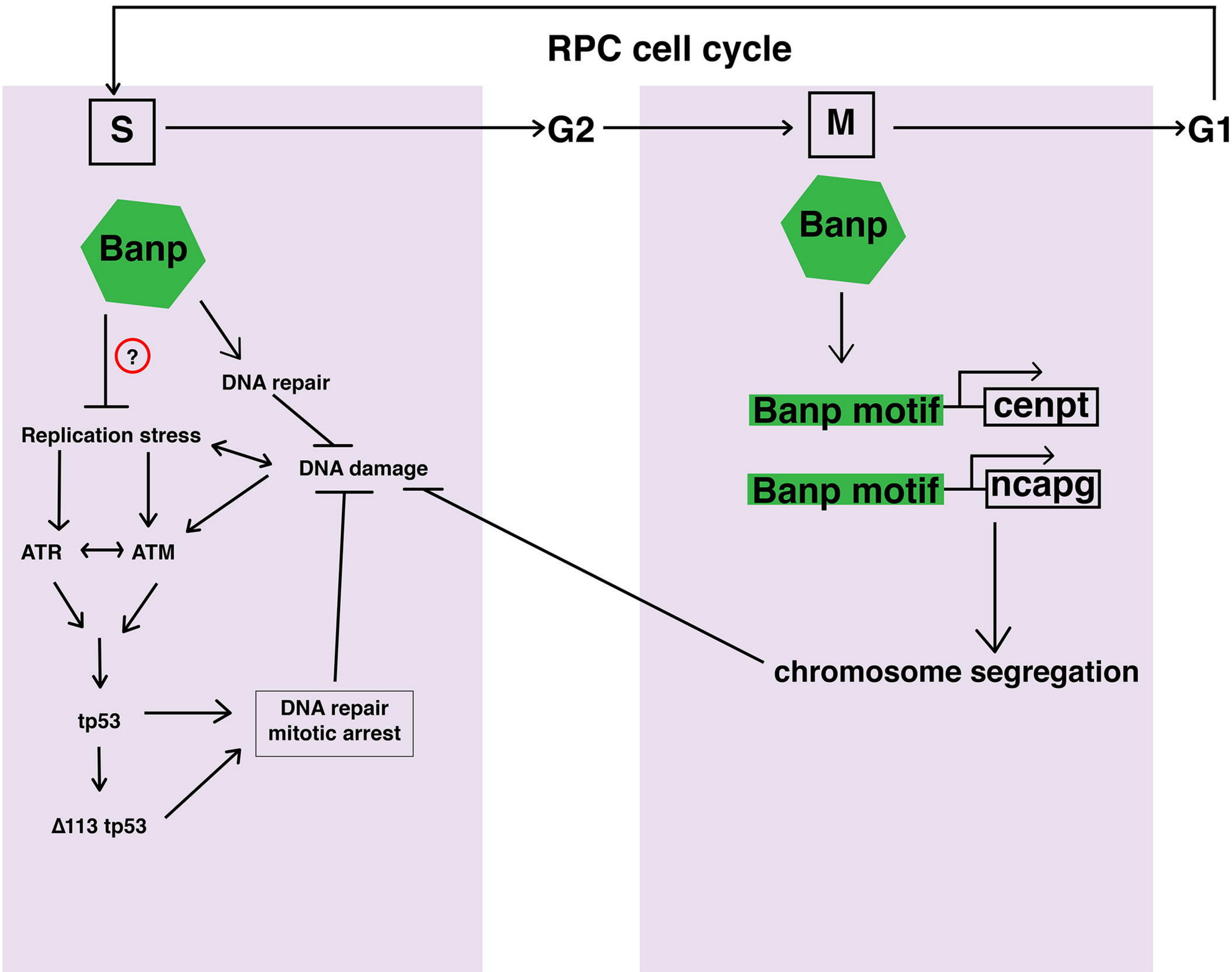
RPC cell cycle
S
G2
M
G1
Banp
?
DNA repair
Replication stress
DNA damage
ATR
ATM
tp53
DNA repair
mitotic arrest
Δ113 tp53
Banp
Banp motif
cenpt
Banp motif
ncapg
chromosome segregation

Figure 7